Magnus effect in General Relativity

Rita Morais Franco

Thesis to obtain the Master of Science Degree in

Engineering Physics

Supervisors: Prof. Vítor Manuel dos Santos Cardoso
Dr. Luís Filipe de Pinho Oliveira e Costa

Examination Committee

Chairperson: Prof. Ana Maria Vergueiro Monteiro Cidade Mourão
Supervisor: Prof. Vítor Manuel dos Santos Cardoso
Member of the Committee: Dr. Christopher James Moore

7th May 2018

Dedicated to my Grandparents

Resumo

O efeito de Magnus em dinâmica de fluidos descreve a força que um corpo em rotação sofre ao mover-se num fluido, sendo esta uma força perpendicular à velocidade e ao eixo de rotação - a força de Magnus. Em relatividade geral, resultados numéricos e previsões teóricas recentes apontavam para a existência de um efeito análogo a este, no sentido da rotação num corpo em movimento criar uma força perpendicular tanto ao eixo de rotação como à velocidade, o que motivou a investigação desta possibilidade.

Nesta tese partimos das equações de um corpo rotativo a mover-se num campo gravitacional e deduzimos o que chamámos de efeito "Magnus" gravitacional. Também deduzimos um efeito "Magnus" electromagnético. O gravitoelectromagnetismo serve como ligação entre as duas áreas.

Consideremos um corpo em rotação movendo-se num meio. A força de Magnus gravitacional surge quando a velocidade relativa entre o corpo e o meio não é paralela ao spin do objecto. De forma análoga ao efeito de Magnus clássico, esta força é ortogonal a densidade de corrente espacial e ao eixo de rotação do corpo. Para o caso gravitacional, a força aponta no mesmo sentido da força de Magnus clássica; no caso electromagnético depende da carga do objecto, apontando no sentido oposto para uma carga positiva.

Este fenómeno é estudado em diferentes sistemas astrofísicos de interesse, nomeadamente um corpo em rotação: no espaço-tempo descrito pela métrica FLWR e numa "nuvem" de matéria escura.

Alguns resultados desta Dissertação, entre outros, podem ser encontrados na Ref. [1].

Palavras-chave: efeito de Magnus, força de spin-curvatura, tensores de maré, relatividade geral, gravitoelectromagnetismo.

Abstract

The fluid dynamics Magnus effect is a well studied phenomenon, describing the change in the expected trajectory of a body due to its rotation. A spinning body moving in a fluid suffers a force orthogonal to both the body's velocity and axis of rotation - the Magnus force. In General Relativity, numerical results and theoretical predictions hinted at the existence of an analogous effect, in the sense that a moving rotating body will suffer a force orthogonal to both its velocity and axis of rotation, and motivated us to investigate this possibility.

In this thesis we start from the equations for a spinning body moving in a gravitational field and deduce what we dubbed the gravitational “Magnus” effect. We also show the existence of electromagnetic Magnus effect. Gravitoelectromagnetism is used to establish a comparison between the two areas.

Take a spinning body moving in a medium. The gravitational Magnus force arises whenever the relative velocity between the body and the medium is non-parallel to the body's spin. In an analogous way to the classical effect, this force is orthogonal to the spatial mass-energy current density and to the body's axis of rotation. In gravitation, it points in the same direction of the classical effect; while in electromagnetism it depends on the object's charge, pointing in the opposite direction for a positive charge.

This phenomenon is studied in different astrophysical systems, namely a spinning body in the FLWR spacetime, and a dark matter halo.

Some of the results of this thesis, among others, can be found in Ref. [1].

Keywords: Magnus effect, spin-curvature force, tidal tensors, general relativity, gravitoelectromagnetism.

Contents

List of Figures

Notation and Convention

- Metric signature is $(-+++)$.
- $c = G = 1$ where c is the speed of light in vacuum and G is the gravitational constant, unless specified.
- Greek letters $\alpha, \beta, \gamma, \cdots$ denote 4D spacetime indices, running 0-3 while Roman letters $i, j, k, ...$ denote spatial indices running 1-3.
- $\epsilon_{\alpha\beta\sigma\gamma} \equiv \sqrt{-g}[\alpha\beta\sigma\gamma]$ is the Levi-Civita tensor, with the orientation $[1230] = 1$, i.e., in flat spacetime $\epsilon_{1230} = 1$.
- The convention for the Riemann tensor is $R^{\alpha}_{\beta\mu\nu} = \Gamma^{\alpha}_{\beta\mu,\nu} - \Gamma^{\alpha}_{\beta\nu,\mu} + ...$
- $\star$ denotes the Hodge dual: for an antisymmetric tensor $F_{\alpha\beta} = F_{[\alpha\beta]}$, $\star F_{\alpha\beta} \equiv \frac{1}{2}\epsilon_{\alpha\beta}{}^{\mu\nu} F_{\mu\nu}$.
- Bold simbols denote 3-vectors: $\boldsymbol{A} = A_i = (A_1, A_2, A_3)$.

BH	Black Hole
DM	Dark matter
EFE	Einstein field equations
EM	Electromagnetism
FLRW	Friedmann-Lemaître-Robertson-Walker [metric]
GEM	Gravitoelectromagnetism
GR	General Relativity
GW	Gravitational Wave

Chapter 1

Introduction

1.1 Overview and Motivation

1.1.1 Gravitational background

A gravitational problem is usually simpler in Newtonian physics than in General Relativity (GR). Take for example a system of two point masses whose only interaction is due to the gravitational potential. In classical mechanics, this exercise can always be reduced to a two one-body equivalent problem. However, in a relativistic description of gravity, this is not possible anymore since matter, curvature of the spacetime, and its manifestation - gravity - can no longer be dissociated. Spacetime tells matter how to move and mass tells spacetime how to curve and gravity "is not a foreign and physical force transmitted through space and time. It is a manifestation of the curvature of spacetime" [2]. This is in agreement with Mach's statements: *M1. The matter distribution determines the geometry* [3]. The field equations for gravity, also called the Einstein Field Equations (EFE), have this characteristic imprinted on them, by relating the geometric Einstein tensor $G_{\alpha\beta} \equiv R_{\alpha\beta} - 1/2Rg_{\alpha\beta}$ (itself related to the spacetime through the metric) and the energy-momentum tensor $T_{\alpha\beta}$ that encodes the description of matter [4]:

$$G_{\alpha\beta} = \kappa T_{\alpha\beta} \, , \tag{1.1}$$

where $\kappa = 8\pi$ is called the coupling constant. These equations are rather difficult to solve, and usually do not have an exact solution.

The N-body problem originated the post-Newtonian (PN) approximation theory, a useful method to study the Einstein field equations, assuming a slow motion condition $v \ll c$ and weak field approximation. It amounts to obtain the equations of motion of a system up to a power of small parameters (v^2/c^2, GM/r or other combinations) [4–6]. It measures the order of deviation from the Newtonian theory [2]. Throughout this thesis, we shall use the parametrization of Ref. [7], expanding in terms of a dimensionless parameter ϵ, such that $U \sim \epsilon^2$ and $v \lesssim c$, U being the Newtonian potential. Keeping terms up to 1 PN order means keeping terms up to the order of ϵ^4, i.e., $\mathcal{O}(\epsilon^4) \equiv \mathcal{O}(4)$.

This approximation can be used when studying motion of bodies where the gravitational interaction between them is weak. It is still a good approximation even if the bodies are compact, and so strongly self gravitating, as long as the condition of weak gravitation interaction holds.

The 1PN approximation is useful when studying the comparison between electromagnetism and gravitation, particularly in the slow motion approximation and for weak fields. This formalism is called Gravitoelectromagnetism (GEM). Several works on this topic have been developed throughout the years [6–17]. In 1961, the linearized equations of GR were used to pose a comparison between GR and EM without using tensor formalism, except to deduce the linearized equations [9]. The 1PN approximation was used in a Maxwell-like form as a tool to study particular celestial systems [7, 10]. In 1972, it was studied the analogy between the force applied on a magnetic dipole in an electromagnetic field and the force applied on a gyroscope in a gravitational field [11]. An analogy using the exact GEM fields defined in the 1+3 formalism [12] was made in 2007 [14]. Another approach was later cast in 2008 [15], by expressing the forces not in terms of the GEM fields directly, but in terms of tidal tensors; this approach was proven to be exact and *covariant* [15, 16]. It was also shown that for the motion of spinning test particles in a gravitational field (whose equations of motion are the Mathisson-Papapetrou equations [18, 19] under the Mathisson Pirani spin condition) exact GEM analogies emerge [16]. The analogy between the precession of magnetic dipole in an electromagnetic field and of the gyroscope in a gravitational field had already been studied by many authors [2, 20] in a linear approximation to GR. Some analogies have been cast in Refs. [12, 14, 17], without the need of using approximations.

In the GEM formalism, we can write the Einstein field equations in an analogous form to the Maxwell's equations, by introducing the 1PN gravitoelectric and gravitomagnetic fields [7, 10]

$$\boldsymbol{G} = \nabla w - \dot{\boldsymbol{A}} + \mathcal{O}(6)\,, \qquad\qquad \boldsymbol{H} = [\boldsymbol{\nabla} \times \boldsymbol{A}] + \mathcal{O}(5)\,, \tag{1.2}$$

denoting the scalar $w = U + \mathcal{O}(U^2) = U + \mathcal{O}(4)$ and the 3-vector A_i as the "gravitomagnetic vector potential", that is $\mathcal{O}(3)$ [7].

In gravity, a spinning body produces a gravitomagnetic field that deflects flow particles (like its magnetic analogue), thus suggesting a Magnus-like force. This field is not physical like the magnetic field, depending on the chosen reference frame [17]. The gravitomagnetic field is in fact the relativistic Coriolis field [21].

1.1.2 Applications

As previously stated, a lot of analogies and comparisons can be made between GR and EM. A particular interesting similarity is that both Maxwell's equations from electromagnetism and Einstein field equation from gravitation have radiative solutions. In fact, in a weak field approximation, one can check that in GR perturbation waves are produced (analogue to the electromagnetic waves for the Maxwell's equations). These Gravitational Waves (GW) are perturbations of the curvature that propagate in spacetime [2, 3, 5]. Einstein was the first to find this solution for the linearized field equations. He also pointed that the amplitude of these waves would be incredibly small [22, 23]. The physical existence of GW was disputed for decades, with Einstein himself changing his position several times.

In 1975 the first binary pulsar system, PSR B1913+16, was discovered, which allowed a continuous study of a binary neutron star system [24]. Years of data acquisition revealed that the rate of decay of the orbital period was consistent with the energy loss through GW emission [25]. A Nobel prize was awarded to Hulse and Taylor in 1993 for this discovery and analysis, as it not only provided a new test and confirmation of the GR theory but also opened a new field of study of gravitation [26]. Gravitational waves emission provides important information of the astrophysical system that emitted them, and so we could use them to test different theories.

The search for the gravitational wave signals would continue for quite a few years. They were first detected in 2015 by the LIGO Scientific Collaboration and Virgo Collaboration [27], produced by the merger of a binary BH system. With the detection of more GW signals [28, 29], it was possible to detect one from a binary neutron star merger [29]. A second Nobel Prize in Physics in 2017 was awarded to the field of gravitational waves, this time for its detection, to Rainer Weiss, Kip Thorne and Barry Barish [30].

Although gravitational waves are becoming one of the most attractive methods to detect new gravitational effects, there are also different contexts which may prove useful to signal possible new phenomena. In this case, one such scenario to study different effects is the exact solution of the Einstein field equations assuming a perfectly homogeneous isotropic spacetime. This is described by the Friedmann-Lemaître-Robertson-Walker (FLRW) metric:

$$ds^2 = -dt^2 + a^2(t)\left[\frac{dr^2}{1-kr} + r^2\left(d\theta^2 + \sin^2\theta d\phi^2\right)\right], \tag{1.3}$$

here written in terms of spherical coordinates [3, 4, 31–34]. In this formula, $k \in \{-1, 0, 1\}$ is a constant related with the curvature of space, and $a(t)$ is the scale function. The values $k = -1$ and $k = 0$ represent negative or zero spatial curvature and translate into an infinite (open) Universe, while $k = +1$ represents positive spatial curvature, hence a finite (closed) Universe [2, 3, 5, 35].

In standard cosmology, the FLRW metric, derived in 1922, is used as a background model [5, 36].

Metrics that obey the Friedmann equations, given by

$$\frac{\dot{a}(t)^2 + k}{a(t)^2} = \frac{8\pi\rho + \Lambda}{3}, \tag{1.4}$$

$$-\frac{\ddot{a}(t)}{a(t)} = \frac{4\pi}{3}(\rho + 3p) - \frac{\Lambda}{3}, \tag{1.5}$$

define the FLRW universes [35]. The study of this metric is motivated by the cosmological principle which states that the Universe is homogeneous and isotropic with the exception of local deviations [3]. This means that it has no privileged points or directions and is seen as the same everywhere and from every direction. This is remarkably close to what we observe. On a very large scale of $10^8 - 10^9$ light-years, the Universe is observed to be homogeneous [2, 5]. We also verify isotropy in the distribution of galaxies on a large scale, in the value of the Hubble constant on a very large scale, and at a smaller scales in the cosmic X-ray background and the cosmic microwave background (up to a few parts in 10^{-5}) [2].

So far, the Universe seems remarkably flat (i.e. $k = 0$), as several experiments show. However, the amount of mass in the Universe is not compatible with a flat spacetime. To satisfy the flat geometry, mass

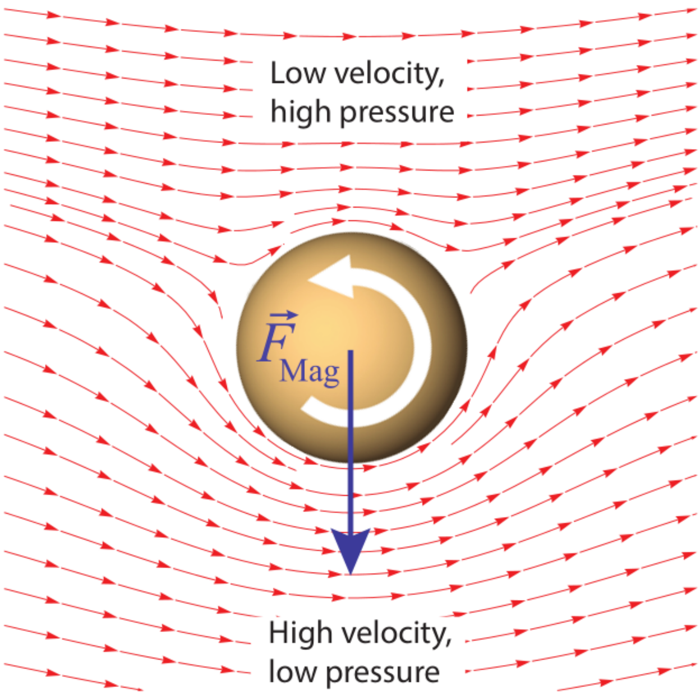

Figure 1.1: Rotating body moving in a fluid. On the top part of the body, its velocity will slow down the fluid, while in the bottom it will speed up the fluid. This causes a pressure difference, that leads to the Magnus force, pointing downwards (orthogonal both to the body's rotation axis and velocity).

density must be $\sim$ 100 bigger than that currently observed [5]. This missing density was attributed to Dark Matter (DM) and Dark Energy, that are theorized forms of matter and energy that do not interact with electromagnetic radiation the way ordinary matter does and we only know of its existence through its gravitational effects. The first hint of the existence of such a form of matter was the observed velocity dispersion curve of stars around the galaxy [37]. The curve suggested that the mass of the galaxies had to be much larger than the estimated mass from stellar observations. Other observational evidences were given throughout the years, namely the velocity dispersion of galaxies in a cluster around its center, gravitational lensing and the anisotropies of the cosmic microwave background, among others [38–42].

Dark energy was mainly proposed to justify the accelaration of the expansion of the Universe. This form of energy seemed to interact with the Universe as a whole, without local effects (like DM for example) [43]. Dark energy is usually modeled through the cosmological constant (as it was also introduced to justify for the expansion of the Universe). The nature of DM and dark energy is still a mistery.

To account for the observed expansion, DM should make up to about 27% of the Universe, as opposed to the 5% of ordinary matter. The majority of the mass-energy density content, the other 68%, is dark energy [44].

1.1.3 Classical Magnus effect

The classical Magnus effect is a well-known phenomenon in our everyday life, describing the change in the expected trajectory of an object due to its rotation, in the presence of a fluid [45]. It was described as it is for the first time in 1852 by Heinrich Magnus [46].

To understand the physics behind the classical phenomenon, consider a rotating body in a homogeneous non-compressible fluid that has a constant flow, much like a football moving through the air, see Fig. 1.1. The body's rotation slows down the fluid on one side and increases its velocity on the other side, and as we can see by the Bernoulli equation (neglecting gravity) [45],

$$p + \frac{1}{2}\rho v^2 = \text{const}, \tag{1.6}$$

this leads to a pressure difference between the two sides of the body that causes a force, sometimes called the *lift* force, normal to the stream. This force depends on the medium's density, the body's spin, the relative velocity between the medium and the body, and the dimensions/geometry of the body: $\boldsymbol{F} \propto \rho \boldsymbol{\omega} \times \boldsymbol{v}$.

The Magnus effect is noticeable in several sports, take the example of a curved ball in football, baseball, but also cricket or golf [47]. In the realm of ballistic, the effect was also widely investigated, to better predict the trajectory of shells mortars of different sizes and shapes. This effect has some engineering applications in the design of motors for very specific types of ships and airplanes. These motors, invented in the 1920s, are typically consisted of cylinders powered by a motor. In particular, the rotor/Flettner ships have a large ($\sim$ 19m of height and 3m of diameter) vertical cylinders that create a pressure difference in the air around and hence a Magnus force capable of moving the ship [48].

The contact surface between the body and the fluid is essential to the Magnus effect. This casts doubts on the possibility of such an effect in gravitational problems, since BH do not have a surface.

The suggestion of a Magnus-like force in GR was suggested by numerical results published in 1999 [49]. In 2014, theoretical arguments were given for the existence of a similar force, based on the fact that a spinning black hole accretes more matter in one side than on the other [50]. This force, however, had an opposite direction than the classical one. In 2016, there was also an attempt to demonstrate the existence of an effect, and the force suggested also pointed in the direction opposite to the Magnus effect [51].

1.2 Thesis Outline

This thesis is mainly divided into three parts. The first one (Chapter 2) is dedicated to electromagnetism, namely providing an example of an ”electromagnetic Magnus force”, and gravitoelectromagnetism, by deriving the 1PN GEM equations. It also shows the similarities and differences between EM and GR and elucidates how one could make analogous arguments to the electromagnetic case even in a gravitational problem. The second part is the most important, as it lays the foundation of this work. In this part, Chapter 3, we start from the Mathisson-Papapetrou equations of motion for a spinning body in General Relativity. We show, without approximations that the spin-curvature force naturally splits into two components, one of them being the gravitational Magnus force. The 1PN approximation is also addressed, allowing us to study an example similar to the one discussed in Chapter 2. Finally, in Chapter 4, we develop some applications of the Magnus force on two astrophysical systems: a spinning particle in a FLWR background, and a spinning particle in a DM Halo.

Chapter 2

Electromagnetic Magnus Effect

In this chapter we start by considering what we call an electromagnetic analogue (in terms of behavior, not in terms of its origin, or essence) of the classical Magnus effect. It will give some intuition when we later study the gravitational analogue of this effect. We also deduce the 1PN Gravitoelectromagnetic equations.

2.1 Electromagnetic example

Consider a magnetic dipole (of magnetic moment 4-vector μ^α, 4-velocity U^α and 4-momentum P^α) inside a current slab, as depicted in Fig. 2.1. The force exerted on the dipole placed in an EM field described by a Faraday tensor $F^{\alpha\beta}$ can be covariantly written as [16]

$$\frac{DP^\alpha}{d\tau} = F^\alpha_{\mathrm{EM}} = B^{\beta\alpha}\mu_\beta, \tag{2.1}$$

$$B_{\alpha\beta} = \star F_{\alpha\nu;\beta}U^\nu = \frac{1}{2}\epsilon_{\alpha\nu}{}^{\mu\rho}F_{\mu\rho;\beta}U^\nu, \tag{2.2}$$

where $B_{\alpha\beta}$ is the magnetic tidal tensor and $\star$ denotes the Hodge dual. The magnetic tidal tensor encodes magnetic tidal effects measured by an observer comoving with the magnetic dipole. This tensor equals the covariant derivative of the magnetic field $B^\alpha = \star F^{\alpha\beta}U_\beta$ as measured in the inertial frame comoving with the particle. In the inertial frame comoving with the particle, the spatial components of F^α_{EM} of (2.1) yield the textbook expression:

$$\boldsymbol{F}_{\mathrm{EM}} = \nabla(\boldsymbol{B}\cdot\boldsymbol{\mu}). \tag{2.3}$$

It is useful to decompose $B_{\alpha\beta}$ into its symmetric and antisymmentric parts:

$$B_{\alpha\beta} = B_{(\alpha\beta)} + B_{[\alpha\beta]}\,.$$

If we take the projection orthogonal to U^α of the Maxwell field equations,

$$F^{\alpha\beta}{}_{;\beta} = 4\pi j^\alpha\,, \tag{2.4}$$

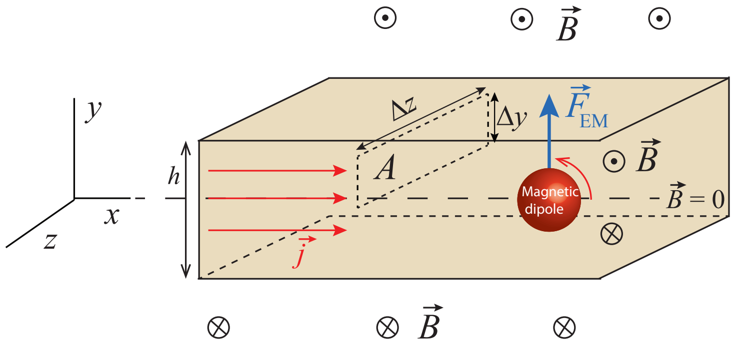

Figure 2.1: A magnetic dipole $\boldsymbol{\mu} = \mu \boldsymbol{e}_z$ inside a current slab (a semi-infinite cloud of charged particles flowing in one direction). The slab is finite in the y direction, and infinite in the x and z directions. The dipole suffers a force $\boldsymbol{F}_{\text{EM}} = 4\pi j \mu \boldsymbol{e}_y$. In this case $\boldsymbol{F}_{\text{Mag}} = \boldsymbol{F}_{\text{sym}}$, and so the force is twice the Magnus force ($\boldsymbol{F}_{\text{EM}} = \boldsymbol{F}_{\text{sym}} + \boldsymbol{F}_{\text{Mag}} = 2\boldsymbol{F}_{\text{Mag}}$). If we consider instead a slab finite in the z direction and infinite in the x and y directions, keeping the magnetic dipole $\boldsymbol{\mu} = \mu \boldsymbol{e}_z$, the Magnus force remains the same $\boldsymbol{F}_{\text{Mag}} = 2\pi j \mu \boldsymbol{e}_y$, but the $\boldsymbol{F}_{\text{sym}}$ now points in the opposite direction: $\boldsymbol{F}_{\text{EM}} = -2\pi j \mu \boldsymbol{e}_y = -\boldsymbol{F}_{\text{Mag}}$. This leads to a total EM force: $\boldsymbol{F}_{\text{EM}} = 0$.

(where j^α is the current density 4-vector), we find [16]

$$B_{[\alpha\beta]} = \frac{1}{2} \star F_{\alpha\beta;\gamma} U^\gamma - 2\pi \epsilon_{\alpha\beta\sigma\gamma} j^\sigma \,. \tag{2.5}$$

The first term of Eq.(2.5) is related to the laws of EM induction, while the second is a current term. This decomposition of the magnetic tidal tensor allows us to write the total EM force as the sum of three different contributions: the symmetric force, the current force and the induction force, i.e.,

$$F^\alpha_{\text{EM}} = F^\alpha_{\text{sym}} + F^\alpha_{\text{Mag}} + F^\alpha_{\text{ind}} \,, \tag{2.6}$$

$$F^\alpha_{\text{sym}} = B^{(\alpha\beta)} \mu_\beta \,, \tag{2.7}$$

$$F^\alpha_{\text{ind}} = -\frac{1}{2} \star F^{\alpha\beta}{}_{;\gamma} U^\gamma \mu_\beta \,, \tag{2.8}$$

$$F^\alpha_{\text{Mag}} = 2\pi \epsilon^\alpha_{\ \beta\sigma\gamma} U^\gamma j^\sigma \mu^\beta \,. \tag{2.9}$$

Let us analyze the force F^α_{Mag}. It is a force orthogonal to the magnetic moment μ^α and to the charge current relative to the dipole $h^\alpha_\beta j^\beta$. In the particle's rest frame, $\mu^\alpha = (0, \boldsymbol{\mu})$ and the Magnus force reduces to its spatial components as the time component vanishes:

$$\boldsymbol{F}_{\text{Mag}} = 2\pi \boldsymbol{\mu} \times \boldsymbol{j}. \tag{2.10}$$

Here it is obvious that the force is orthogonal both to $\boldsymbol{\mu}$ and $\boldsymbol{j}$. For a magnetic dipole consisting of a spinning charged body, the direction of the magnetic moment will depend on the charge: for a positive charge, $\boldsymbol{\mu} \parallel \boldsymbol{S}$ and $\boldsymbol{F}_{\text{Mag}}$ has the opposite direction of the classical Magnus force (so it is actually "anti-Magnus"); for a negative charge, $\boldsymbol{\mu} \parallel -\boldsymbol{S}$ and $\boldsymbol{F}_{\text{Mag}}$ has the same direction of the classical Magnus force. The induction component of the force exerted on a magnetic dipole placed in a EM field does not have a gravitational analogue and so it is not of particular relevance to us.

Considering the setup of a current slab, infinite in the x and z direction and of finite thickness h

along y (a slab delimited by the planes $y = -h/2$ and $y = h/2$), with $\boldsymbol{j}$ on the positive x direction. This exercise is similar to Exercise 5.14 of Ref. [52]. By the right-hand rule, we know the magnetic field will point to the $\boldsymbol{e}_z$ direction for $y > 0$ and to $\boldsymbol{e}_z$ for $y < 0$. For the plane $y = 0$, $\boldsymbol{B} = 0$. The magnetic field can be found by applying the Ampère's law

$$\nabla \times \boldsymbol{B} = 4\pi \boldsymbol{j}\,, \tag{2.11}$$

to the amperian loop A depicted Fig. 2.1: a rectangle perpendicular to the x direction, of boundary ∂A and normal unit vector $\boldsymbol{n}$, that we take to be $\boldsymbol{n} \parallel \boldsymbol{j}$. By the Stokes theorem, we have that

$$\oint_{\partial A} \boldsymbol{B} \cdot d\boldsymbol{l} = \oint_A \nabla \times \boldsymbol{B} \cdot \boldsymbol{n} dA = 4\pi \oint_A \boldsymbol{j} \cdot \boldsymbol{n} dA = 4\pi \Delta z \Delta y\,, \tag{2.12}$$

and on the other hand, $\oint_{\partial A} \boldsymbol{B} \cdot d\boldsymbol{l} = B(y)\Delta z$. This means that $B^z = 4\pi \Delta y j$, and so the magnetic field inside the slab ($y < h/2$) is

$$B^z = 4\pi y j\,, \tag{2.13}$$

and outside the slab ($y > h/2$) is

$$B^z = 2\pi h j\,. \tag{2.14}$$

Hence the only non-vanishing component of the magnetic tidal tensor defined in (2.2) is $B^{zy} = 4\pi j$. This means that F^α_{EM} in (2.1) will be

$$\boldsymbol{F}_{\mathrm{EM}} = B^{zy} \mu_z \boldsymbol{e}_y = 4\pi j \mu_z \boldsymbol{e}_y = \boldsymbol{F}_{\mathrm{Mag}} + \boldsymbol{F}_{\mathrm{sym}}. \tag{2.15}$$

This configuration is stationary so $\boldsymbol{F}_{\mathrm{ind}} = 0$. Explicitly, $\boldsymbol{F}_{\mathrm{Mag}}$ and $\boldsymbol{F}_{\mathrm{sym}}$ are given by

$$\boldsymbol{F}_{\mathrm{Mag}} = 2\pi \boldsymbol{\mu} \times \boldsymbol{j} = 2\pi j (\mu_z \boldsymbol{e}_y - \mu_y \boldsymbol{e}_z)\,, \tag{2.16}$$

$$\boldsymbol{F}_{\mathrm{sym}} = B^{(ji)} \mu_j \boldsymbol{e}_i = 2\pi j (\mu_z \boldsymbol{e}_y - \mu_y \boldsymbol{e}_z). \tag{2.17}$$

Now fix the direction of the dipole $\boldsymbol{\mu} = \mu \boldsymbol{e}_z$ and analyze the forces (2.16) and (2.17) for different slab orientations. Considering a

1. Slab finite along y and infinite in the x and z direction, as the one in Fig. 2.1, the magnetic field is along the z direction and we have

$$\boldsymbol{F}_{\mathrm{Mag}} = \boldsymbol{F}_{\mathrm{sym}} = 2\pi j \mu \boldsymbol{e}_y \qquad \Rightarrow \qquad \boldsymbol{F}_{\mathrm{EM}} = 2\boldsymbol{F}_{\mathrm{Mag}} = 4\pi j \mu \boldsymbol{e}_y.$$

2. Slab finite along z and infinite in the x and y direction, the magnetic field is now along y ($\boldsymbol{B} = -4\pi j z \boldsymbol{e}_y$), and so the only non-vanishing component of $B^{\alpha\beta}$ is $B^{yz} = -4\pi j$. This causes the symmetric part of the magnetic tidal tensor, i.e., $B^{(ij)}$ to change its sign when compared to the

previous example; hence

$$\boldsymbol{F}_{\text{Mag}} = -\boldsymbol{F}_{\text{sym}} = -2\pi j \mu \boldsymbol{e}_z \qquad \Rightarrow \qquad \boldsymbol{F}_{\text{EM}} = 0.$$

Notice how the Magnus force $\boldsymbol{F}_{\text{Mag}}$ remains the same in both cases, being the symmetric force that changes to the exact opposite. This leads to two very different total forces in both examples. Notice also that for other orientations of the slab and dipole the Magnus and Weyl forces are not collinear. They usually have some component in the same direction, except when $\boldsymbol{\mu}$ coincides with an eigenvector of $B^{(ij)}$ where the forces are orthogonal. For the orientation of the slab depicted in Fig. 2.1, this happens when $\boldsymbol{\mu} = \frac{\mu}{\sqrt{2}}(\boldsymbol{e}_y + \boldsymbol{e}_z)$ or $\boldsymbol{\mu} = \frac{\mu}{\sqrt{2}}(\boldsymbol{e}_z - \boldsymbol{e}_y)$; $\boldsymbol{\mu} = \mu \boldsymbol{e}_x$ also coincides with an eigenvector but it has zero eigenvalues and so $\boldsymbol{F}_{\text{Mag}} = \boldsymbol{F}_{\text{Sym}} = 0$.

Another important remark is that the forces do not depend on the width h of the cloud/slab; in fact, the only purpose of considering a finite dimension to the cloud is to provide boundary conditions for the computation of the direction of the magnetic field. A cloud infinite in all directions would lead to an undetermined problem.

2.2 Derivation of GEM equations in 1PN approximation

Post-Newtonian theory can be formulated in various different forms [4, 7, 10, 53]. Here we will use the dimensionless parameter ϵ such that $U \sim \epsilon^2$ and $v \lesssim \epsilon$ where U is minus the Newtonian potential and v the bodies' velocity. The first post-Newtonian order (1PN) amounts to keep terms up to $\mathcal{O}(\epsilon^4) \equiv \mathcal{O}(4)$.

We are using the same parametrization of Ref. [7], denoting the scalar $w = U + \mathcal{O}(U^2) = U + \mathcal{O}(4)$ and the 3-vector A_i that is $\mathcal{O}(3)$. Our metric is:

$$g_{00} = -\exp(-2w) = -1 + 2w - 2w^2 + \mathcal{O}(6); \tag{2.18}$$

$$g_{0i} = A_i + \mathcal{O}(5); \tag{2.19}$$

$$g_{ij} = \delta_{ij} \exp(+2w) = \delta_{ij}(1 + 2U) + \mathcal{O}(4). \tag{2.20}$$

The Christoffel symbols up to $\mathcal{O}(4)$ are:

$$\Gamma^0_{00} = -\dot{U} + \mathcal{O}(5); \tag{2.21}$$

$$\Gamma^0_{0i} = -U_{,i} + \mathcal{O}(4); \tag{2.22}$$

$$\Gamma^i_{00} = \dot{\mathcal{A}}_i - w_{,i} + 4UU_{,i} + \mathcal{O}(6); \tag{2.23}$$

$$\Gamma^i_{0j} = \delta_{ij}\dot{U} + \frac{1}{2}(A_{i,j} - A_{j,i}) + \mathcal{O}(5); \tag{2.24}$$

$$\Gamma^0_{ij} = -\frac{1}{2}(\mathcal{A}_{i,j} + \mathcal{A}_{j,i}) + \delta_{ij}\dot{w} + \mathcal{O}(5); \tag{2.25}$$

$$\Gamma^i_{jk} = (1 - 2U)(\delta_{ik}U_{,j} + \delta_{ij}U_{,k} - \delta_{jk}U_{,i}) + \mathcal{O}(6). \tag{2.26}$$

The Riemann tensor is then defined using these connection coefficients [54]

$$R^{\alpha}_{\beta\gamma\delta} = \partial_\gamma \Gamma^{\alpha}_{\beta\delta} - \partial_\delta \Gamma^{\alpha}_{\beta\gamma} + \Gamma^{\alpha}_{\mu\gamma}\Gamma^{\mu}_{\beta\delta} - \Gamma^{\alpha}_{\mu\delta}\Gamma^{\mu}_{\beta\gamma}. \tag{2.27}$$

The Ricci tensor is the contraction of the Riemann tensor, $R_{\beta\delta} = R^{\alpha}_{\beta\alpha\delta}$ [54].

We now introduce the 1PN *gravitoelectric field* $\mathbf{G}$ and *gravitomagnetic field* $\mathbf{H}$, defined like [7, 10]

$$\boldsymbol{G} = \nabla w - \dot{\boldsymbol{A}} + \mathcal{O}(6); \qquad \boldsymbol{H} = [\boldsymbol{\nabla} \times \boldsymbol{A}] + \mathcal{O}(5). \tag{2.28}$$

From this definitions alone, we get two Maxwell-like equations:

$$\nabla \times \mathbf{G} = -\dot{\boldsymbol{H}} + \mathcal{O}(6), \tag{2.29}$$

$$\nabla \cdot \mathbf{H} = \mathcal{O}(4). \tag{2.30}$$

The Einstein field equations are [3]

$$G_{\alpha\beta} = \kappa T_{\alpha\beta}\,, \tag{2.31}$$

where $G_{\alpha\beta} \equiv R_{\alpha\beta} - 1/2 R g_{\alpha\beta}$ is the Einstein tensor, $\kappa = 8\pi$ is called the coupling constant and $T_{\alpha\beta}$ is the energy-momentum tensor. The Einstein equations may also be written in a different way, using the trace of the energy-momentum tensor, $T \equiv T^{\alpha}_{\alpha}$:

$$R^{\alpha\beta} = 8\pi \left(T^{\alpha\beta} - \frac{1}{2} T g^{\alpha\beta} \right) . \tag{2.32}$$

Let $\rho = T^{\alpha\beta} u_\alpha u_\beta$ and $J^\alpha = -T^{\alpha\beta} u_\beta$ be, respectively, the mass-energy density and current density as measured by the observers u^α. Here $T^{\alpha\beta}$ is the stress energy tensor. For dust, this tensor is given by $T^{\alpha\beta} = \rho_0 u^\alpha u^\beta$, in non-relativistic units, with $\rho_0 = \rho_0(x)$ being the proper density. From the relation $\nabla^2 U \simeq -4\pi\rho$ (Gauss' law) we infer that ρ is of order $\mathcal{O}(2)$. We then have $T^{00} = \rho + O(4)$, $T^{0i} = J^i + O(5) \sim O(3)$, where we noted that $J^i \sim \rho v_{\mathrm{matter}} \sim O(3)$, and $T^{ij} \sim O(4)$. Noting also that $T^{\gamma}_{\ \gamma} = T^{0}_{\ 0} + T^{i}_{\ i} = T^{00} g_{00} + T^{ii} + O(6)$, we obtain the Ricci tensor components

$$R_{00} = -4\pi (T^{00} + T^{ii}) + O(6); \tag{2.33}$$

$$R_{0i} = -8\pi J_i + O(5); \tag{2.34}$$

$$R_{ij} = 4\pi\rho\delta_{ij} + O(4). \tag{2.35}$$

On the other hand, computing explicitly the components of the Ricci tensor using the Christoffel symbols in Eqs. (2.21) to (2.26), yields

$$R_{00} = -\nabla \cdot \boldsymbol{G} - 3\frac{\partial^2 U}{\partial t^2} + O(6)\,, \tag{2.36}$$

$$R_{0i} = \frac{1}{2}(\nabla \times H)_i - 2\frac{\partial \boldsymbol{G}}{\partial t} + O(5)\,, \tag{2.37}$$

$$R_{ij} = -\delta_{ij} \nabla \cdot \boldsymbol{G} + O(4)\,. \tag{2.38}$$

Equating Eqs. (2.33)-(2.35) to (2.36)-(2.38) we obtain (cf. Eqs. (3.22) of [10], or Eqs. (2.6) of [7])

$$\nabla \cdot \boldsymbol{G} = -4\pi(T^{00} + T^{ii}) - 3\frac{\partial^2 U}{\partial t^2} + O(6)\,, \tag{2.39}$$

$$\nabla \times \boldsymbol{H} = -16\pi \boldsymbol{J} + 4\frac{\partial \boldsymbol{G}}{\partial t} + \mathcal{O}(5)\,, \tag{2.40}$$

with the third equation, coming from R_{ij}, being redundant as it is already contained in the first. These equations are analogous to two of the Maxwell equations of electromagnetism: the Gauss law $\nabla \cdot \boldsymbol{E} = 4\pi\rho_c$, and the Maxwell-Ampère law $\nabla \times \boldsymbol{B} = 4\pi\boldsymbol{j} + \partial_t \boldsymbol{E}$.

The similarity between the gravitomagnetic equation and the Maxwell's equations provides an efficient way to predict and investigate new gravitational effects, by making a direct bridge with an extensively studied area of Electromagnetism. This idea will be explored further in the next chapter.

Chapter 3

Gravitational Magnus effect

In this chapter we investigate the motion of a spinning body in a gravitational field, and determine the forces that this body is subjected to, due to its spin. Finally, we compute the forces that the body will be subjected to up to 1 PN order. We then compute the specific example of a spinning body placed in a (moving) cloud of particles.

3.1 Gravitational Magnus effect

A classical non-spinning test particle, if only subjected to gravitational forces, will follow a geodesic. A spinning particle, however, when placed in a gravitational field, will suffer the spin-curvature force that deviates the particle from its geodesic motion. This spinning particle will be described by the 4-velocity U^α, 4-momentum P^α and the spin-tensor $S^{\mu\nu}$. These last two are related to the energy-momentum tensor $T^{\alpha\beta}$; for the precise definitions we refer to [16, 55, 56]. From the conservation equations $\nabla_\beta T^{\alpha\beta} = 0$, we get the equations of motion [16, 18, 19]:

$$\frac{DP^\alpha}{d\tau} = -\frac{1}{2} R^\alpha_{\beta\mu\nu} S^{\mu\nu} U^\beta \equiv F^\alpha; \tag{3.1}$$

$$\frac{DS^{\alpha\beta}}{d\tau} = 2P^{[\alpha} U^{\beta]}. \tag{3.2}$$

These are called the Mathisson-Papapetrou equations, describing the motion of a spinning body in a gravitational field. We can close the system (3.1)-(3.2) (note that it has 10 independent equations and 13 unkown variables) by introducing a spin condition $S_{\alpha\beta}u^\beta = 0$, for some timelike unit vector u^α. The physical meaning for this extra equation is to specify the frame where the center of mass (CM) of the body is to be evaluated, since for a spinning body the later depends on the observer [16]. Here, we will use the Mathisson-Pirani spin condition:

$$S^{\alpha\beta} U_\beta = 0, \tag{3.3}$$

corresponding to taking $u^\beta = U^\beta$ ($U^\alpha = \mathrm{d}x^\alpha/\mathrm{d}\tau$), meaning that the CM is being measured in its own rest frame [16]. With this spin condition, we may write

$$S^{\mu\nu} = \epsilon^{\mu\nu\tau\lambda} S_\tau U_\lambda, \tag{3.4}$$

where S_α is the spin 1-form, which in the body's CM rest frame has components $(0, \mathbf{S})$ [16]. Substituting on Eq. (3.1), we obtain an expression for the spin-curvature force

$$\frac{DP^\alpha}{d\tau} \equiv -\mathbb{H}^{\beta\alpha} S_\beta \,, \tag{3.5}$$

$$\mathbb{H}_{\alpha\beta} \equiv \star R_{\alpha\mu\beta\nu} U^\mu U^\nu = \frac{1}{2}\epsilon_{\alpha\mu}{}^{\lambda\tau} R_{\lambda\tau\beta\nu} U^\mu U^\nu \,, \tag{3.6}$$

in terms of the gravitomagnetic tidal tensor $\mathbb{H}_{\alpha\beta}$, the so called magnetic part of the Riemann tensor, measured by an observer comoving with the particle.

Comparing Eq. (2.1) with Eq. (3.5), we see the physical analogy between force exerted on a magnetic dipole in a current slab and the gravitational spin-curvature force. Also, $\mathbb{H}_{\alpha\beta}$ is the gravitational analogue of $B_{\alpha\beta}$.

In similarity with the method used for the magnetic tidal tensor $B_{\alpha\beta}$, Eq. (2.2), we now decompose $\mathbb{H}_{\alpha\beta}$ into its symmetric and antisymmetric parts. We use the definition of the Weyl tensor in four dimensions [3]:

$$C_{\alpha\beta\gamma\delta} = R_{\alpha\beta\gamma\delta} + \frac{1}{2}(g_{\alpha\delta}R_{\gamma\beta} + g_{\beta\gamma}R_{\delta\alpha} - g_{\alpha\gamma}R_{\delta\beta} - g_{\beta\delta}R_{\gamma\alpha}) + \frac{1}{6}(g_{\alpha\gamma}g_{\delta\beta} - g_{\alpha\delta}g_{\gamma\beta})R \,, \tag{3.7}$$

or, written compactly,

$$R^{\alpha\beta}{}_{\gamma\delta} = C^{\alpha\beta}{}_{\gamma\delta} + 2\delta^{[\alpha}_{[\gamma} R^{\beta]}{}_{\delta]} - \frac{1}{3} R \delta^{\alpha}_{[\gamma}\delta^{\beta}_{\delta]} \,. \tag{3.8}$$

We can then write the gravitomagnetic tidal tensor as

$$\mathbb{H}_{\alpha\beta} = \star C_{\alpha\mu\beta\nu} U^\nu U^\mu - 4\pi\epsilon_{\alpha\beta\sigma\gamma} J^\sigma U^\gamma \equiv \mathcal{H}_{\alpha\beta} - 4\pi\epsilon_{\alpha\beta\sigma\gamma} J^\sigma U^\gamma \,, \tag{3.9}$$

where we defined $\mathcal{H}_{\alpha\beta} = \mathbb{H}_{(\alpha\beta)} = \star C_{\alpha\mu\beta\nu} U^\nu U^\mu$ (magnetic part of the Weyl tensor) [57], and $J^\alpha = -T^{\alpha\beta} U_\beta$ is the mass/energy current 4-vector as measured by an observer of 4-velocity U^α [16]. Thus, we divide the spin-curvature force into two parts:

$$F^\alpha = -\mathcal{H}^{\alpha\beta} S_\beta + 4\pi\epsilon^\alpha{}_{\beta\sigma\gamma} J^\beta S^\sigma U^\gamma = F^\alpha_{\mathrm{Weyl}} + F^\alpha_{\mathrm{Mag}} \,, \tag{3.10}$$

$$F^\alpha_{\mathrm{Weyl}} \equiv -\mathcal{H}^{\alpha\beta} S_\beta \,, \tag{3.11}$$

$$F^\alpha_{\mathrm{Mag}} \equiv -\mathbb{H}_{[\alpha\beta]} S_\beta \equiv 4\pi\epsilon^\alpha{}_{\beta\sigma\gamma} J^\beta S^\sigma U^\gamma \,. \tag{3.12}$$

Note that F^α_{Weyl} is somewhat analogous to F^α_{sym} of EM, defined in Eq. (2.7), and that there is no induction term. The term F^α_{Mag} is the one with most physical relevance to us. F^α_{Mag} arises whenever there is a spatial mass current $h^\alpha{}_\beta J^\beta$ relative to the body not parallel to spin 4-vector S^α. Here $h^\alpha{}_\beta \equiv \delta^\alpha{}_\beta + U^\alpha U_\beta$

is the space projector orthogonal to U^α. In the particle's rest frame,

$$\boldsymbol{F}_{\text{Mag}} = 4\pi \boldsymbol{J} \times \boldsymbol{S}. \tag{3.13}$$

We call this force the gravitational analogue to the Magnus effect in fluid dynamics due to its similarities, since:

- it arises whenever the body is rotating and moving in a medium with a relative velocity not parallel to the spin axis ($\boldsymbol{J} \nparallel \boldsymbol{S}$);
- it is orthogonal both to the spin and the current density, and it has the same direction of the classical Magnus force.

F^α_{Mag} solely depends on U^α, $h^\alpha{}_\beta J^\beta$ and S^α; while F^α_{Weyl} is strongly dependent on details of the system, and may have any direction. This can be traced back to the fact that F^α_{Mag} comes from the Ricci part of the curvature, totally fixed by the energy momentum-tensor $T^{\alpha\beta}$ of the local sources via the Einstein equations (2.32), whereas the Weyl tensor does not couple to the sources via algebraic equations , only through differential ones (differential Bianchi identities), being thus determined not by $T^{\alpha\beta}$ at a point, but by conditions elsewhere.

3.1.1 Post-Newtonian approximation

Using the 1PN metric (2.19) previously introduced, the relevant components of the gravitomagnetic tidal tensor can be determined up to 1PN:

$$\mathbb{H}_{00} = \mathcal{O}(5)\,, \tag{3.14}$$

$$\mathbb{H}_{0i} = \frac{1}{2}\epsilon_j{}^{lk} A_{k,li} v^j + \epsilon_{ij}{}^l \dot{U}_l v^j + \mathcal{O}(5)\,, \tag{3.15}$$

$$\mathbb{H}_{ij} = -\frac{1}{2}\epsilon_i{}^{lk} \mathcal{A}_{k,lj} - \epsilon_{ij}{}^k \dot{U}_{,k} + 2\epsilon_i{}^{km} v_k U_{,jm} + \mathcal{O}(5)\,. \tag{3.16}$$

We only need the spatial components, since $F^j = -\mathbb{H}^{\alpha j} S_\alpha = -\mathbb{H}^{ij} S_i - \mathbb{H}^{0j} S_0 = -\mathbb{H}^{ij} S_i + \mathcal{O}(\epsilon^5)$. Rewriting Eq. (3.16) in terms of the gravitomagnetic and gravitoelectric fields:

$$\mathbb{H}_{ij} = -\frac{1}{2} H_{i,j} - \epsilon_{ijk} \dot{G}^k + 2\epsilon_{ik}{}^m v^k G_{j,m} - \epsilon_{ij}{}^m v^k G_{j,m} + \mathcal{O}(5)\,, \tag{3.17}$$

$$\tag{3.18}$$

Finally we can write the 1PN spin-curvature force and its Weyl and Magnus components as:

$$F^j = \frac{1}{2} H^{i,j} S_i - \left[\boldsymbol{S} \times \dot{\boldsymbol{G}}\right]^j - 2\epsilon^i{}_{km} v^k G^{j,m} S_i - \epsilon^{jim} v^k G_{k,m} S_i\,, \tag{3.19}$$

$$F^i_{\text{Weyl}} = \frac{1}{2} H^{(i,j)} S_j - 2\epsilon^{(i}{}_{km} G^{j)}{}_{,m} v^k S_j + \mathcal{O}(5)\,, \tag{3.20}$$

$$F^i_{\text{Mag}} = 4\pi \epsilon^i{}_{jk} S^k (T^{0j} - \rho v^j) + \mathcal{O}(5)\,. \tag{3.21}$$

A spinning body in a gravitational field will not only suffer the spin-curvature force, but also the inertial “force” already present in the geodesic motion. This may be derived from the usual geodesic equation for a point-like non-spinning particle in a gravitational field [3]:

$$\frac{DU^\alpha}{d\tau} = 0 \Leftrightarrow \frac{d^2x^\alpha}{d\tau^2} + \Gamma^\alpha_{\beta\gamma} U^\beta U^\gamma = 0\,. \tag{3.22}$$

Using $d/d\tau = (dt/d\tau)d/dt$ in order to express the previous equation in terms of t, we obtain

$$\frac{d^2t}{d\tau^2}\frac{dx^\alpha}{dt} + \left(\frac{dt}{d\tau}\right)^2 \left(\frac{d^2x^\alpha}{dt^2} + \Gamma^\alpha_{\beta\gamma}\frac{dx^\beta}{dt}\frac{dx^\gamma}{dt}\right) = 0\,. \tag{3.23}$$

Since $x^0 = t \Rightarrow \frac{d^2t}{d\tau^2} = \frac{d^2x^0}{d\tau^2}$ we can use Eq. (3.22) to write:

$$\frac{d^2x^0}{d\tau^2} = -\Gamma^0_{\beta\gamma}\frac{dx^\beta}{d\tau}\frac{dx^\gamma}{d\tau} = -\Gamma^0_{\beta\gamma}\left(\frac{dt}{d\tau}\right)^2\frac{dx^\beta}{dt}\frac{dx^\gamma}{dt}\,, \tag{3.24}$$

and substitute it in (3.23) to obtain finally

$$\frac{d^2x^\alpha}{dt^2} + \left(\Gamma^\alpha_{\beta\gamma} - \frac{1}{c}\Gamma^0_{\beta\gamma}\frac{dx^\beta}{dt}\frac{dx^\gamma}{dt}\right)\frac{dx^\beta}{dt}\frac{dx^\gamma}{dt} = 0. \tag{3.25}$$

The time component vanishes trivially, and for the spatial components are responsible for the inertial force, giving

$$\frac{d^2x^i}{dt^2} = \frac{F^i_{\mathrm{I}}}{m_0} = -\left(\Gamma^i_{\beta\gamma} - \frac{1}{c}\Gamma^0_{\beta\gamma}\frac{dx^i}{dt}\right)\frac{dx^\beta}{dt}\frac{dx^\gamma}{dt}\,, \tag{3.26}$$

or, up to 1PN,

$$\boldsymbol{F}_{\mathrm{I}} = (1 + v^2 - 2U)\boldsymbol{G} + \boldsymbol{v}\times\boldsymbol{H} - (3\dot{U} + 4\boldsymbol{G}\cdot\boldsymbol{v})\boldsymbol{v}\,. \tag{3.27}$$

3.1.2 GEM analogue of EM case

We will now investigate the gravitational analogue of the electromagnetic example of Section 2.1: a spinning body inside a medium flowing in the x direction. This medium is assumed to be infinite in the x and z directions and of finite thickness h in the y direction (contained within the planes $-h/2 \leqslant y \leqslant h/2$) as shown in Fig. 3.1.

Since this setup is stationary we have $\nabla\times\boldsymbol{H} = -16\pi\boldsymbol{J}$, where $J^\alpha = -T^{\alpha\beta}u_\beta$ is the mass-energy current as measured by the reference observers $u^\alpha = u^0\delta^\alpha_0$. To obtain the gravitomagnetic field in this example, we can use an analogous reasoning to the one leading to the magnetic field of Eq. (2.13), resulting in

$$\boldsymbol{H} = H^z(y)\boldsymbol{e}_z = -16\pi y J\boldsymbol{e}_z\,. \tag{3.28}$$

Notice how similar it is to the magnetic field of Eq. (2.13), apart from the different factor and opposite sign. The gravitomagnetic tidal tensor has only 1 non-zero component: $\mathbb{H}^{zy} = 8\pi J$. The 1PN spin-curvature force (3.19) for a spinning body at rest in a stationary gravitational field is

$$F_{\mathrm{GSC}} = \frac{1}{2}H^{j,i}S_j \Leftrightarrow \boldsymbol{F}_{\mathrm{GSC}} = \frac{1}{2}\nabla(\boldsymbol{H}\cdot\boldsymbol{S})\,, \tag{3.29}$$

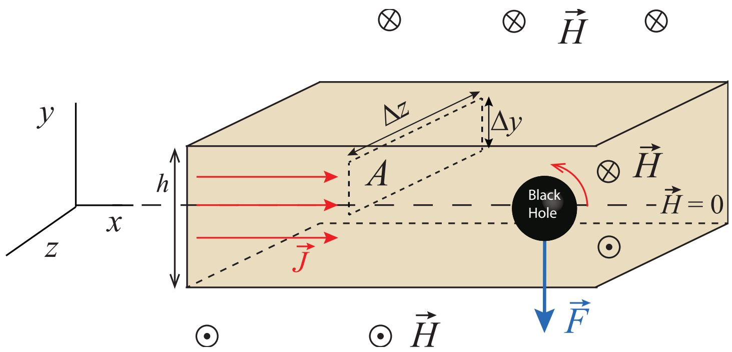

Figure 3.1: A spinning particle (that could be a BH, for example) inside a massive cloud flowing in one direction. The cloud is finite in the y direction, and infinite in the x and z directions. The particle suffers a force $\boldsymbol{F} = -8\pi J S \boldsymbol{e}_y$. In this case $\boldsymbol{F}_{\rm Mag} = \boldsymbol{F}_{\rm Weyl}$, and so the force is twice the Magnus force ($\boldsymbol{F} = \boldsymbol{F}_{\rm Weyl} + \boldsymbol{F}_{\rm Mag} = 2\boldsymbol{F}_{\rm Mag}$). If we consider instead a cloud finite in the z direction and infinite in the x and y directions, keeping the spin of the particle $\boldsymbol{S} = S\boldsymbol{e}_z$, the Magnus force remains the same $\boldsymbol{F}_{\rm Mag} = -4\pi J S\boldsymbol{e}_y$, but the $\boldsymbol{F}_{\rm Weyl}$ now points in the opposite direction: $\boldsymbol{F}_{\rm Weyl} = 4\pi J S \boldsymbol{e}_y = -\boldsymbol{F}_{\rm Mag}$. This leads to a total force: $\boldsymbol{F} = 0$.

that is, once again, similar to the force in Eq. (2.1). Explicitly, the force exerted on the spinning body is:

$$\boldsymbol{F} = -8\pi J S_z \boldsymbol{e}_y \,. \tag{3.30}$$

This force is along the y direction, pointing in the same direction of the classical Magnus effect. The symmetric part of the $\mathbb{H}^{ij}$ is $\mathbb{H}^{ij} = 4\pi J$. The Magnus and Weyl forces are, respectively:

$$\boldsymbol{F}_{\rm Mag} = 4\pi \boldsymbol{J} \times \boldsymbol{S} = 4\pi J (S_y \boldsymbol{e}_z - S_z \boldsymbol{e}_y)\,, \tag{3.31}$$

$$\boldsymbol{F}_{\rm Weyl} = -\mathcal{H}^{ij}\mu_j \boldsymbol{e}_i - 4\pi J (S_z \boldsymbol{e}_y + S_y \boldsymbol{e}_z)\,. \tag{3.32}$$

This is for a fixed orientation of the slab and arbitrary $\boldsymbol{S}$; but this is physically equivalent to considering a fixed $\boldsymbol{S}$ and varying the orientation of the slab. Two notable cases arise, choosing $\boldsymbol{S} = S\boldsymbol{e}_z$:

1. Cloud finite along y (like the one displayed in Fig. 3.1): As seen, $\boldsymbol{H} = -16\pi J y \boldsymbol{e}_z$ and so the only non-vannishing component of the gravitomagnetic tidal tensor is $\mathbb{H}^{zy} = 8\pi j$, leading to $\mathcal{H}^{yz} = 4\pi j$. In this case:

$$\boldsymbol{F}_{\rm Mag} = \boldsymbol{F}_{\rm Weyl} = -4\pi J S \boldsymbol{e}_y \qquad \Rightarrow \qquad \boldsymbol{F} = 2\boldsymbol{F}_{\rm Mag} = -8\pi J S \boldsymbol{e}_y \,. \tag{3.33}$$

2. Cloud finite along z: The gravitomagnetic field is now $\boldsymbol{H} = 16\pi J z \boldsymbol{e}_y$, hence $\mathbb{H}^{yz} = -8\pi J$ and $\mathcal{H}^{ij} = -4\pi J$. In this example, the Magnus force remains the same as in case 3.1.2; however the Weyl force changes sign:

$$\boldsymbol{F}_{\rm Weyl} = -\boldsymbol{F}_{\rm Mag} = 4\pi J S \boldsymbol{e}_y \qquad \Rightarrow \qquad \boldsymbol{F} = \boldsymbol{F}_{\rm Mag} + \boldsymbol{F}_{\rm Weyl} = 0. \tag{3.34}$$

As in the electromagnetic example, we see that $\boldsymbol{F}_{\rm Mag}$ remains the same in both configurations, while $\boldsymbol{F}_{\rm Weyl}$ depends on the details of the system (in this case the boundary conditions of the slab).

Chapter 4

Applications

In this chapter, we study the Magnus force in different situations. Firstly, we present an exact example, with cosmological applications, secondly we compute, for two astrophysical examples, the approximated forces derived in the previous chapter.

4.1 FLRW

As stated in Eq. (1.3), the FLRW metric is given by:

$$ds^2 = -dt^2 + a^2(t)\left(\frac{dr^2}{1-kr^2} + r^2 d\theta^2 + r^2 \sin^2\theta d\phi^2\right) . \tag{4.1}$$

This metric is conformally flat, i.e. there is a non-zero differentiable function $\Omega(\boldsymbol{x})$ such that $g_{\alpha\beta} = \Omega^2(\boldsymbol{x})\eta_{\alpha\beta}$ where $\eta_{\alpha\beta}$ is the Minkowsky metric. Consequently, its Weyl tensor vanishes: $C_{\alpha\beta\gamma\delta} = 0$ [3], which means the Weyl force is zero in this context. It is a particularly interesting case, since the total spin-curvature force exerted on a spinning body in the FLWR spacetime is reduced to the Magnus force:

$$F^\alpha = F^\alpha_{\text{Mag}} . \tag{4.2}$$

For an arbitrary observer with $U^\alpha = U_0(1, \boldsymbol{v}) = \frac{dt}{d\tau}(1, v^i)$, the only non-vanishing components of the gravitomagnetic tensor are

$$\mathbb{H}_{ij} = \mathbb{H}_{[ij]} = \epsilon_{ijk0} v^k A(t, r, \theta) , \tag{4.3}$$

where we define

$$A(t, r, \theta) \equiv \frac{(U^0)^2}{a^2(t)}\left[k + \dot{a}(t)^2 - a(t)\ddot{a}(t)\right] . \tag{4.4}$$

The gravitomagnetic tidal tensor reduces to its anti-symmetric part: the current term that originates the Magnus force.

If the observer is at rest ($\boldsymbol{v} = \boldsymbol{0}$) with the coordinate system of (1.3), its gravitomagnetic tidal tensor vanishes $\mathbb{H}_{\alpha\beta} = 0$. Therefore the the spin curvature force on the spinning body also vanishes: $F^\alpha_{\text{cloud,body}} = -\mathbb{H}^{\beta\alpha} S_\beta = 0$. This was expected from Eq.(3.13), since the spinning body is comoving with the backgroung fluid, so the spatial mass/current $\boldsymbol{J}$ relative to the background is zero, leading to a vanishing Magnus force.

For an observer with peculiar velocity, $\boldsymbol{v} \neq \mathbf{0}$, i.e. an observer moving with respect to the coordinate system of (1.3), the gravitomagnetic tidal tensor (4.3) is not zero. Hence a spinning body moving with velocity v suffers a spin-curvature force given by:

$$F^0 = -\mathbb{H}^{0\alpha} S_\alpha = 0, \tag{4.5}$$

$$F^i = -\mathbb{H}^{i\alpha} S_\alpha = -\mathbb{H}^{ia} S_a = -[\boldsymbol{v} \times \boldsymbol{S}]^i \frac{(U^0)^2}{a^2(t)} [k + \dot{a}(t)^2 - a(t)\ddot{a}(t)], \tag{4.6}$$

$$\boldsymbol{F} = A(t, r, \theta)[\boldsymbol{S} \times \boldsymbol{v}], \tag{4.7}$$

written in terms of the metric parameters.

The stress-energy tensor that corresponds to the metric (1.3) is that of a perfect fluid:

$$T^{\alpha\beta} = (\rho + p) u^\alpha u^\beta + p g^{\alpha\beta} .$$

Hence the mass energy tensor is:

$$J^\alpha = -T^{\alpha\beta} U_\beta = \gamma(\rho + p) u^\alpha - p U^\alpha , \tag{4.8}$$

with $\gamma \equiv -u_\alpha U^\alpha$. Substituting Eq. (4.8) in the expression for the spin-curvature force 4.2, we write

$$F^\alpha = +\mathbb{H}^{\alpha\beta} S_\beta \tag{4.9}$$

$$= 4\pi \epsilon^\alpha{}_{\beta\sigma\gamma} U^\gamma \gamma (\rho + p) u^\beta . \tag{4.10}$$

Since the fluid is at rest in the coordinate system of (1.3), we have $u^\alpha = \delta^\alpha_0$ and $\gamma = -(-\delta^0_\alpha) U^\alpha = U^0$. This leads to:

$$\begin{aligned} F^\alpha_{\text{cloud,body}} &= 4\pi\gamma(\rho + p) \epsilon^\alpha{}_{\beta\sigma\gamma} \delta^\beta_0 S^\sigma U^\gamma \\ &= 4\pi\gamma(\rho + p) \epsilon^\alpha{}_{\sigma\gamma 0} S^\sigma U^\gamma , \end{aligned}$$

from which we can see that the time component of the force is zero and the spatial components read:

$$\boldsymbol{F} = -4\pi (U^0)^2 (\rho + p) [\boldsymbol{v} \times \boldsymbol{S}] . \tag{4.11}$$

One can check that Eq. (4.7) leads in fact to Eq. (4.11) using the Friedmann equations[3],

$$\frac{\dot{a}(t)^2 + k}{a(t)^2} = \frac{8\pi\rho + \Lambda}{3} , \tag{4.12}$$

$$-\frac{\ddot{a}(t)}{a(t)} = \frac{4\pi}{3}(\rho + 3p) - \frac{\Lambda}{3} . \tag{4.13}$$

Let us analize the expression 4.11. For the general case that $\rho + p \neq 0$, a spinning body arbitrarily

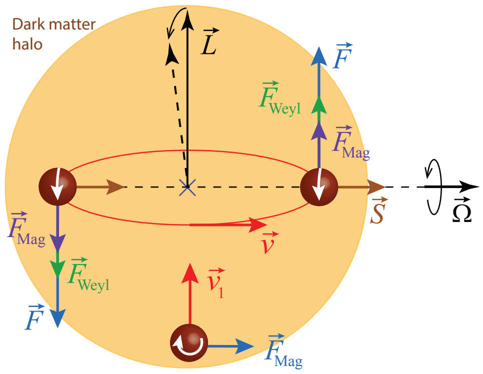

Figure 4.1: Spinning particles moving in a pseudo-isothermal DM halo. For a spinning body in a quasi-circular orbit, with spin lying in the orbital plane, the Magnus and Weyl forces are parallel ($\boldsymbol{F}_{\text{Weyl}} \parallel \boldsymbol{F}_{\text{Magnus}}$). The total force is of the form $\boldsymbol{F} = A(r)\boldsymbol{S} \times \boldsymbol{v}$. The orbital plane will precess with angular velocity Ω, since the total force $\boldsymbol{F}$ points outwards the orbital plane in half the orbit and inwards the other half. For a simplified scheme of this secular orbital precession, see Fig. 4.3. For a body moving radially towards the center of the halo, the Weyl force is null ($\boldsymbol{F}_{\text{Weyl}} = 0$) and the total force is reduced to the Magnus force ($\boldsymbol{F} = \boldsymbol{F}_{\text{Magnus}} = 4\pi\rho\boldsymbol{S} \times \boldsymbol{v}_1$).

moving in the FLWR metric will always suffer the gravitational Magnus force. Moreover, it is the only force acting on the body, since $\boldsymbol{F}_{\text{Weyl}}$ is zero everywhere. In the particular case of ordinary matter and DM, ρ and p are positive and we have $\boldsymbol{F}$ parallel to $[\boldsymbol{S} \times \boldsymbol{v}]$, pointing in the same direction than the fluid dynamics Magnus effect. For dark energy as modeled by the cosmological constant, $\rho = -p$ and the force vanishes, $\boldsymbol{F} = \boldsymbol{0}$.

The different character of the gravitational Magnus force for different models suggests that this force can be used as a probe for the relation ρ/p, and for the energetic content of the Universe.

4.2 Dark Matter halos

4.2.1 Uniform density Dark Matter halo

We start with a simple example, a sperical DM halo of constant density $\rho = \rho_0$. The gravitoelectric field, to lowest order, equals the Newtonian field:

$$G = \frac{M(r)}{r^3}\boldsymbol{r} = \frac{4\pi\rho_0}{3}, \tag{4.14}$$

where

$$M(r) = \int_0^r \rho(r')d^3r' = \frac{4\pi\rho_0 r^3}{3} \tag{4.15}$$

is the mass enclosed inside a sphere of radius r. The gravitomagnetic tidal tensor as measured by an observer of velocity $\boldsymbol{v}$ is reduced to its antisymmetric part $\mathbb{H}_{ij} = 4\pi\rho_0\epsilon_{ijk}v^k = \mathbb{H}_{[ij]}$. Therefore we know that the Weyl force vanishes for all $\boldsymbol{v}$, $\boldsymbol{F}_{\text{Weyl}} = 0$. The total spin-curvature force felt by a spinning body in this system is:

$$\boldsymbol{F} = \boldsymbol{F}_{\text{Mag}} = 4\pi\rho_0\boldsymbol{S} \times \boldsymbol{v}\,. \tag{4.16}$$

This means that any spinning body moving inside this DM halo will suffer a Magnus force, and it is the only physical force acting on it.

4.2.2 Pseudo isothermal Dark Matter halo

A more realistic model of the density profile of a DM halo is the "pseudo-isothermal" profile given by [58]

$$\rho(r) = \frac{\rho_0}{1+\frac{r^2}{r_c^2}}\,, \tag{4.17}$$

where r_c is the halo core radius and ρ_0 the central halo density. The mass enclosed in a sphere of radius r is then

$$M(r) = \int_0^r \rho(r\prime) d^3 r\prime = 4\pi\rho_0 r_c^2 \left[r - r_c \arctan\left(\frac{r}{r_c}\right)\right]\,. \tag{4.18}$$

The gravitoelectric field is given by

$$\boldsymbol{G} = \frac{-M(r)}{r^3}\boldsymbol{r} = 4\pi\rho_0 r_c^2 \left[r - r_c \arctan\left(\frac{r}{r_c}\right)\right]\boldsymbol{\mathcal{G}}\,, \tag{4.19}$$

where $\boldsymbol{\mathcal{G}} \equiv -\boldsymbol{r}/r^3$ is the Newtonian field per unit mass. The differentiation of $\boldsymbol{G}$ with respect to x^j reads

$$G_{i,j} = 4\pi\rho_0 r_c^2 \left[r - r_c \arctan\left(\frac{r}{r_c}\right)\right]\mathcal{G}_{i,j} - 4\pi\rho\frac{r_i r_j}{r^2}\,,$$

with $\mathcal{G}_{i,j} = -\frac{\delta_{ij}}{r^3} + 3\frac{r_i r_j}{r^5}$.

The gravitomagnetic tidal tensor is given by

$$\mathbb{H}_{ij} = -\left[12\pi\rho_0 r_c^2\left(r - r_c\arctan\frac{r}{r_c}\right)\right]v^k\left(\frac{\epsilon_{ikj}}{r^3} - 2\frac{\epsilon_{ik}{}^m r_j r_m}{r^5} + \frac{\epsilon_{ij}{}^m r_k r_m}{r^5}\right) - \tag{4.20}$$

$$- 2\epsilon_{ik}{}^m v^k\left(4\pi\rho\frac{r_j r_m}{r^2}\right) + \epsilon_{ij}{}^m v^k\left(4\pi\rho\frac{r_k r_m}{r^2}\right) \tag{4.21}$$

$$= -A(r)v^k\left(\frac{\epsilon_{ikj}}{r} - 2\frac{\epsilon_{ik}{}^m r_j r_m}{r^3} + \frac{\epsilon_{ij}{}^m r_k r_m}{r^3}\right) - 2\epsilon_{ik}{}^m v^k\left(4\pi\rho\frac{r_j r_m}{r^2}\right) + \epsilon_{ij}{}^m v^k\left(4\pi\rho\frac{r_k r_m}{r^2}\right)\,, \tag{4.22}$$

$$A(r) \equiv 12\pi\rho_0\frac{r_{\rm c}^2}{r^2}\left[1 - \frac{r_{\rm c}}{r}\arctan\left(\frac{r}{r_{\rm c}}\right)\right]\,. \tag{4.23}$$

For this DM density profile, $\mathbb{H}_{ij}$ is not generically antisymmetric. We decompose it into its symmetric and antisymmetric parts, respectively:

$$\mathcal{H}_{ij} = \mathbb{H}_{(ij)} = 2\frac{A(r) - 4\pi\rho}{r^2}(\boldsymbol{v}\times\boldsymbol{r})_{(i}r_{j)}\,, \tag{4.24}$$

$$\mathbb{H}_{[ij]} = \frac{1}{2}\epsilon_{ijl}\epsilon^{lkm}\mathbb{H}_{km} = 4\pi\rho\epsilon_{ijl}v^l\,. \tag{4.25}$$

Therefore the spin-curvature force that acts on a spinning body moving in this DM halo is

$$\boldsymbol{F} = \boldsymbol{F}_{\text{Weyl}} + \boldsymbol{F}_{\text{Mag}}\,, \tag{4.26}$$

$$F^i_{\text{Weyl}} = -\mathcal{H}^{ij} S_j\,, \tag{4.27}$$

$$\boldsymbol{F}_{\text{Mag}} = 4\pi\rho \boldsymbol{S} \times \boldsymbol{v}\,. \tag{4.28}$$

As we can see, the Magnus force is given by the same expression in the previous uniform DM halo example (4.16), taking into account the changes in the density function. On the other hand, the Weyl force in this density profile DM is usually non-zero, contrasting with the previous uniform density profile, where it vanished for all bodies. Once again the Weyl force demonstrates its heavy dependence on the details of the system.

If the body's velocity is parallel to the body's position ($\boldsymbol{v} \parallel \boldsymbol{r}$), the Weyl force vanishes. Therefore, for a body moving radially, only the Magnus force will act upon it, $\boldsymbol{F} = \boldsymbol{F}_{\text{Mag}}$. However, this only happens initially, as the Magnus force will accelerate the body in a perpendicular direction, and its velocity will no longer be radial.

Objects on quasi-circular orbits

We are interested in the effects of the spin-curvature force on test bodies on circular (or quasi-circular) orbits within the DM halo. This allows the study of interesting phenomena while adopting useful approximations.

The spin evolution equation for a body with orbital angular velocity ω and spin $\boldsymbol{S}$ is [4, 21]

$$\frac{d\boldsymbol{S}}{dt} = \boldsymbol{\Omega}_{\text{s}} \times \boldsymbol{S}\,, \tag{4.29}$$

$$\boldsymbol{\Omega}_{\text{s}} = -\frac{1}{2}\boldsymbol{v} \times \boldsymbol{a} + \frac{3}{2}\boldsymbol{v} \times \boldsymbol{G}\,, \tag{4.30}$$

where $\boldsymbol{\Omega}_{\text{s}}$ is the spin's precession frequency. The first term of $\boldsymbol{\Omega}_{\text{s}}$ is the so-called Thomas precession and the second the geodetic precession. For this setup, the only force acting on the body is the spin-curvature force: $\boldsymbol{a} = \boldsymbol{F}/m$. Hence the Thomas precession is $-\frac{1}{2m}\boldsymbol{v} \times \boldsymbol{F} \sim \mathcal{O}(5)$, negligible to first PN order. Therefore, we can make the approximation

$$\Omega_{\text{s}} \approx \frac{3\boldsymbol{v} \times \boldsymbol{G}}{2}\,. \tag{4.31}$$

Due to the spherical symmetry of the setup, we can choose the orbit to lie in the $x - y$ plane, without loss of generality. The body's velocity will be in the same plane, and is approximately given by

$$\boldsymbol{v} \approx v(-\sin\phi \boldsymbol{e}_x + \cos\phi \boldsymbol{e}_y)\,, \tag{4.32}$$

with $\phi = \omega t$. According to Eq. (4.19), $\boldsymbol{G}$ takes the same direction as the position vector, also along $x - y$ plane and orthogonal to the velocity $\boldsymbol{v}$ since we are considering quasi-circular orbits. Consequently, $\boldsymbol{\Omega}_{\text{s}}$ points in the z direction.

We continue our investigation with extreme cases of the particle's spin orientation: spin in the z direction, and spin with a zero z component, lying in the orbital plane.

1) Spin orthogonal to the orbital plane

We first take the spin to be orthogonal to the orbital plane, i.e. $\boldsymbol{S} = S^z \boldsymbol{e}_z$. The precession frequency is also in the z direction and so we have $\boldsymbol{\Omega}_\mathrm{s} \parallel \boldsymbol{S}$. Therefore, through Eq. (4.29), we know that

$$\frac{d\boldsymbol{S}}{dt} = 0\,, \tag{4.33}$$

consequently the spin remains constant along $\boldsymbol{e}_z$.

The Magnus and Weyl forces read

$$\boldsymbol{F}_\mathrm{Mag} = -4\pi\rho \frac{(\boldsymbol{S}\cdot\boldsymbol{L})}{mr}\boldsymbol{e}_r\,, \tag{4.34}$$

$$\boldsymbol{F}_\mathrm{Weyl} = \boldsymbol{F}_\mathrm{Mag} + A(r)\frac{(\boldsymbol{S}\cdot\boldsymbol{L})}{mr}\boldsymbol{e}_r\,, \tag{4.35}$$

where $\boldsymbol{L}$ is the orbital angular momentum, given by $\boldsymbol{L} = m\boldsymbol{r}\times\boldsymbol{v}$ to lowest order. A simple analysis of the force's expressions leads to the conclusion that

$$\begin{cases} \boldsymbol{F}_\mathrm{Mag} \parallel \boldsymbol{F}_\mathrm{Weyl} & A(r) < 4\pi\rho \\ \boldsymbol{F}_\mathrm{Mag} \parallel -\boldsymbol{F}_\mathrm{Weyl} & A(r) > 4\pi\rho \end{cases}$$

Since the forces are radial, they will only change the effective gravitational attraction, having no other effect on the body's orbit.

2) Spin parallel to the orbital plane

A more intriguing example is to consider the spin to be parallel to the orbital plane in the $(x-y)$ plane. Eq. (4.29) and Eq. (4.30) tell us that $\boldsymbol{S}$ precesses but remains always in $(x-y)$ plane. For an initial $\boldsymbol{S} = S\boldsymbol{e}_x$ and taking into account that $\boldsymbol{\Omega}_\mathrm{s}$ is constant, one can write

$$\boldsymbol{S} = S\left(\cos(\Omega_\mathrm{s}t)\boldsymbol{e}_x + \sin(\Omega_\mathrm{s}t)\boldsymbol{e}_y\right)\,. \tag{4.36}$$

Note that $\boldsymbol{\Omega}_\mathrm{s} \nparallel \boldsymbol{S}$, in fact here $\boldsymbol{\Omega}_\mathrm{s} \perp \boldsymbol{S}$, and so $\frac{d\boldsymbol{S}}{dt}$ is not zero. We will have

$$\boldsymbol{S}\times\boldsymbol{v} = vS\left[\cos(\Omega_\mathrm{s}t)\cos\phi + \sin(\Omega_\mathrm{s}t)\sin\phi\right]\boldsymbol{e}_z \tag{4.37}$$

$$= vS\cos(\phi - \Omega_\mathrm{s}t)\boldsymbol{e}_z = vS\cos[(\omega - \Omega_\mathrm{s})t]\boldsymbol{e}_z\,. \tag{4.38}$$

The Magnus, Weyl and spin-curvature forces that act on the body are given by

$$\boldsymbol{F}_{\text{Mag}} = 4\pi\rho S v \cos[(\omega - \Omega_{\text{s}})t]\boldsymbol{e}_z \,, \tag{4.39}$$

$$\boldsymbol{F}_{\text{Weyl}} = (A(r) - 4\pi\rho) S v \cos[(\omega - \Omega_{\text{s}})t]\boldsymbol{e}_z \,, \tag{4.40}$$

$$\boldsymbol{F} = A(r)\boldsymbol{S} \times \boldsymbol{v} = A(r) S v \cos[(\omega - \Omega_{\text{s}})t]\boldsymbol{e}_z \,. \tag{4.41}$$

All these forces are in the z direction, causing the spinning body to oscillate in this direction along its orbit.

The spin-curvature force (4.41) also gives rise to a precession, although in this case a precession of the orbital plane. The angular momentum, perpendicular to the orbital plane, is given by $\boldsymbol{L} = m\boldsymbol{r} \times \boldsymbol{v}$, to lowest order. Differentiating with respect to time, we obtain

$$\frac{d\boldsymbol{L}}{dt} = m\boldsymbol{r} \times \frac{d\boldsymbol{v}}{dt} \,,$$

and, considering once more that the only force acting on the body is the spin-curvature force, $\frac{d\boldsymbol{v}}{dt} = \frac{d^2\boldsymbol{x}}{dt^2} = \boldsymbol{F}/m$. We have then

$$\frac{d\boldsymbol{L}}{dt} = \boldsymbol{r} \times \boldsymbol{F} = -A(r)\boldsymbol{r} \times [\boldsymbol{v} \times \boldsymbol{S}] \,.$$

We now make use of the vector identity $\boldsymbol{A} \times [\boldsymbol{B} \times \boldsymbol{C}] = [\boldsymbol{A} \times \boldsymbol{B}] \times \boldsymbol{C} + [\boldsymbol{C} \times \boldsymbol{A}]\boldsymbol{B}$, so that

$$\frac{d\boldsymbol{L}}{dt} = A(r)\left[\frac{1}{m}\boldsymbol{S} \times \boldsymbol{L} - (\boldsymbol{S} \times \boldsymbol{r}) \times \boldsymbol{v}\right] \,. \tag{4.42}$$

To extract the contribution of the second term, we average $d\boldsymbol{L}/dt$ along one period:

$$\langle [\boldsymbol{S} \times \boldsymbol{r}] \times \boldsymbol{v} \rangle = A(r)\left[\frac{1}{m}\langle \boldsymbol{S} \times \boldsymbol{L} \rangle - \langle (\boldsymbol{S} \times \boldsymbol{r}) \times \boldsymbol{v} \rangle\right] \tag{4.43}$$

$$= A(r)\left[\frac{1}{m}\boldsymbol{S} \times \boldsymbol{L} - \langle (\boldsymbol{S} \times \boldsymbol{r}) \times \boldsymbol{v} \rangle\right] \,. \tag{4.44}$$

Using Eq. (4.30), one sees that $\Omega_{\text{s}} \sim \omega\epsilon^2$. Typically we have $\omega \gg \Omega_{\text{s}}$ so the spin $\boldsymbol{S}$ (4.30) is nearly constant during one period. Thus, we can assume it constant in a given direction: $\boldsymbol{S} = S\boldsymbol{e}_x$. The first term of Eq. (4.42) is constant along one orbit, and averaging the second term gives

$$\langle [\boldsymbol{S} \times \boldsymbol{r}] \times \boldsymbol{v} \rangle = -Srv \left\langle \sin^2\phi \right\rangle \boldsymbol{e}_y = -\frac{Srv}{2}\boldsymbol{e}_{\boldsymbol{y}} = +\frac{1}{2M}[\boldsymbol{S} \times [\boldsymbol{r} \times \boldsymbol{v}]] = \frac{1}{2M}[\boldsymbol{S} \times \boldsymbol{L}] \,. \tag{4.45}$$

Therefore, the orbital precession can be written as

$$\left\langle \frac{d\boldsymbol{L}}{dt} \right\rangle = \boldsymbol{\Omega} \times \boldsymbol{L}, \tag{4.46}$$

$$\boldsymbol{\Omega} = \frac{A(r)}{2M}\boldsymbol{S} \,, \tag{4.47}$$

where $\boldsymbol{\Omega}$ is the angular velocity of rotation of the orbit's plane. Therefore, we encounter here two different precessions. The object's spin will precess about the z direction, as depicted in Fig. 4.2. The orbit's plane

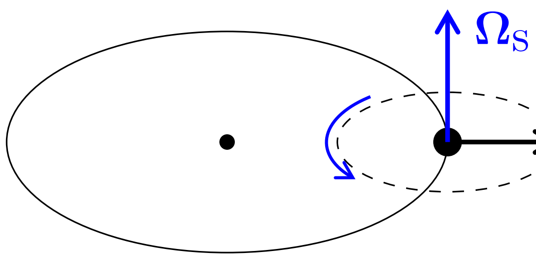

Figure 4.2: Simplified scheme of the precession of the spin $\boldsymbol{S}$ of the particle in a quasi-circular orbit in Fig. 4.1, around $\mathbf{\Omega}_\mathrm{s}$, both in the $x - y$ plane.

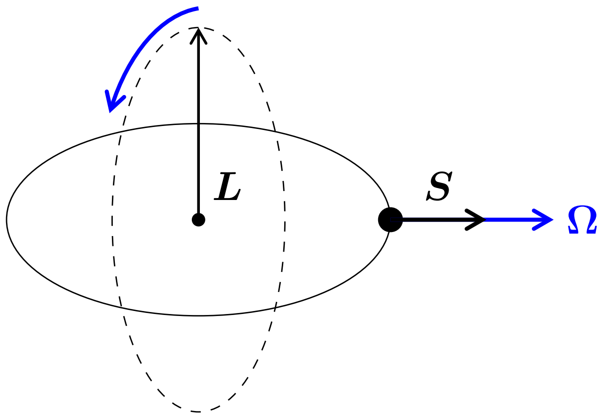

Figure 4.3: Simplified scheme of the precession of the plane of the quasi-circular orbit of the particle in Fig. 4.1. The plane is characterized by $\boldsymbol{L}$ and will precess around $\mathbf{\Omega}$, that is parallel to the particle's spin $\boldsymbol{S}$.

will precess about the direction of the spin, since $\mathbf{\Omega} \parallel \boldsymbol{S}$, see Fig. 4.3. This means the orbit will "tilt". Note, however, that after $t = \pi/\Omega_\mathrm{s}$ the spin's direction will be reversed (due to its own precession), and the orbit will "tilt" to the opposite side.

The evolution equation for the coordinate z is

$$\ddot{z} = \frac{F^z}{M} + G^z \,, \tag{4.48}$$

with G^z being the z component of the gravitational field, acquired by the body when it oscillates out of the plane. We make a first order Taylor expansion about $z = 0$, obtaining

$$G^z \simeq G_{z,z}|_{z=0} z \equiv G_{z,z} z \,, \tag{4.49}$$

with

$$\begin{aligned} G_{z,z} &= 4\pi\rho_0 r_c^2 \left[r - r_c \arctan\left(\frac{r}{r_c}\right)\right] \mathcal{G}_{z,z} - 4\pi\rho \frac{z^2}{r^2} \\ &= -\frac{M(r)}{r^3} = -\omega^2 \,. \end{aligned}$$

The general solution for the differential equation Eq. (4.49) is

$$z(t) = c_1 \cos(\sqrt{-G_{z,z}} t) + c_2 \sin(\sqrt{-G_{z,z}} t) + Z \cos(\Delta\omega t) \,, \tag{4.50}$$

where

$$Z \equiv -\frac{S}{M}\frac{A(r)v}{G_{z,z} + \Delta\omega^2} = \frac{S}{M}\frac{A(r)v}{\Omega_{\rm s}(2\omega - \Omega_{\rm s})}, \tag{4.51}$$

and c_1 and c_2 are arbitrary integration constants. Note that $G_{z,z} < 0$ and $G_{z,z} \neq \Delta\omega \equiv \omega - \Omega_{\rm s}$.

The first two terms of Eq. (4.50) are the solution for $\ddot{z} = G^z$, thus describing the z oscillations of the circular orbit lying off the $x - y$ plane, meaning c_1 and c_2 essentially set up the initial inclination of the orbit. Let us find interesting solutions looking at particular choices of these integration constants.

2a) Constant amplitude regime:

Taking null integration constants ($c_1 = c_2 = 0$) the solution simplifies to

$$z(t) = Z\cos(\Delta\omega t)\,, \tag{4.52}$$

yielding a "bobbing" motion of frequency $\Delta\omega = \omega - \Omega_{\rm s}$ and constant amplitude Z. The particle's trajectory is plotted in Figures 4.4 and 4.5.

We chose $\rho_0 = 5 \times 10^7 M_\odot\ {\rm pc}^{-3}$, a core radius $r_c = 0.02$kpc, and $r = 8r_c$ for which $v = 0.13$, that can happen for a satellite galaxy. For the test body, we chose an object with the $m = M_\odot$, with initial spin vector $\boldsymbol{S}_{\rm in} = S\boldsymbol{e}_x$ with $S = 0.5m^2$. Fig. 4.4 shows the results obtained by approximating $x(t)$ and $y(t)$ coordinates to those of a circular motion of constant radius R, since $z(t) << R$. Therefore plotting:

$$\begin{cases} x(t) = R\cos(\omega t) \\ y(t) = R\sin(\omega t) \\ z(t) = Z\cos(\Delta\omega t) \end{cases} . \tag{4.53}$$

For the results plotted in Fig. 4.5, we solved the equations of motion numerically, i.e., solved the system

$$\frac{d\boldsymbol{S}}{dt} = \boldsymbol{\Omega}_{\rm s} \times \boldsymbol{S}\,, \tag{4.54}$$

$$\frac{d^2\boldsymbol{x}}{dt^2} = \frac{\boldsymbol{F}}{m} + \boldsymbol{G}\,, \tag{4.55}$$

with $\boldsymbol{\Omega}_{\rm s} = -\frac{3}{2}\boldsymbol{v} \times \boldsymbol{G}$.

The test body oscillates between $-Z$ and $+Z$ in each lap, however the plane of the orbit changes in time, meaning that the maximum is reached for different $(x(t), y(t))$ in each lap. The motion can be seen as an orbit with an initial inclination, whose plane precesses with frequency $\Omega_{\rm s}$.

The orbits presented in Figures 4.4 and 4.5 show a remarkable agreement, indicating that the system of equations (4.53) describe well the motion of the particle, despite the approximations used to derive it.

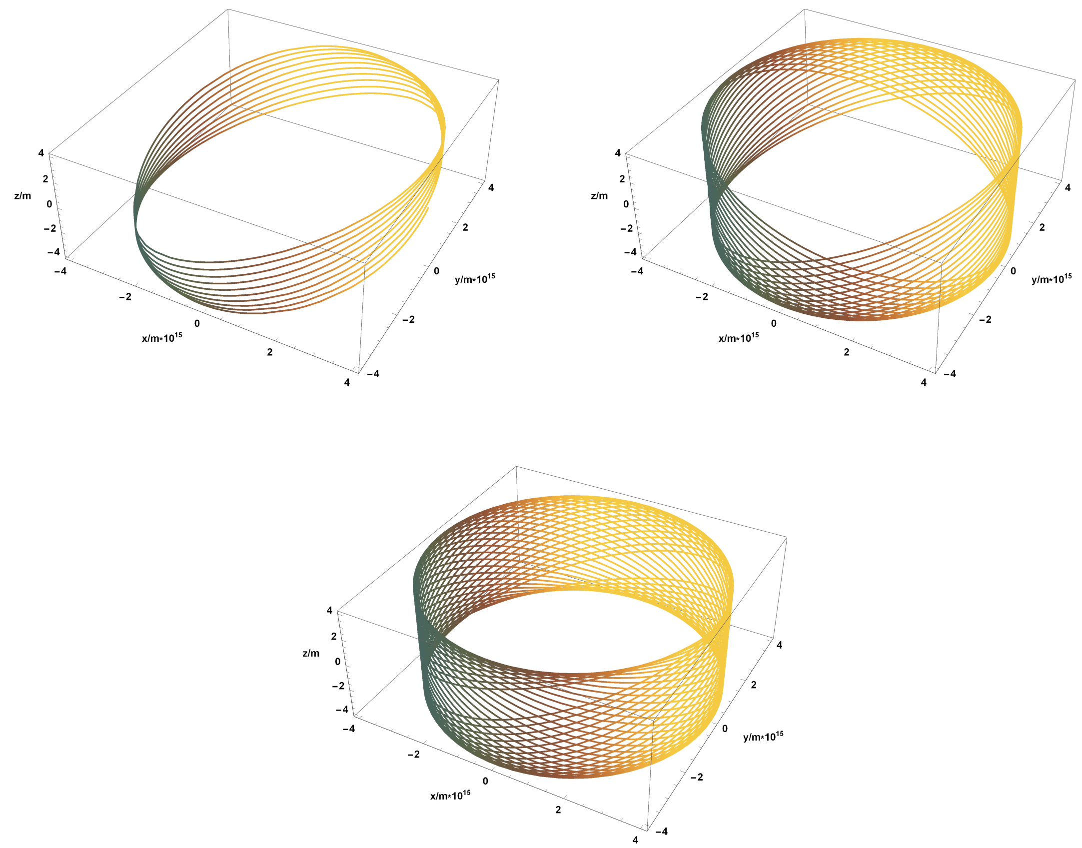

Figure 4.4: Approximated results for a spinning body in a quasi-circular orbits in a pseudo-isothermal dark matter halo, in what we called the constant amplitude regime. The DM halo has $\rho_0 = 5\times10^7 M_\odot/\mathrm{pc}^3$ and $r_c = 0.02$kpc. The test body is located at $r = 8r_c$ (for which $v = 0.13$) and has $m = M_\odot$ and an initial spin vector with magnitude $S = 0.5m^2$ pointing in the $\boldsymbol{e}_\mathrm{x}$ direction. *From left to right, up down*: Plots of $\{x(t), y(t), z(t)\}$ of the orbit, after $10, 25, 40$ laps.

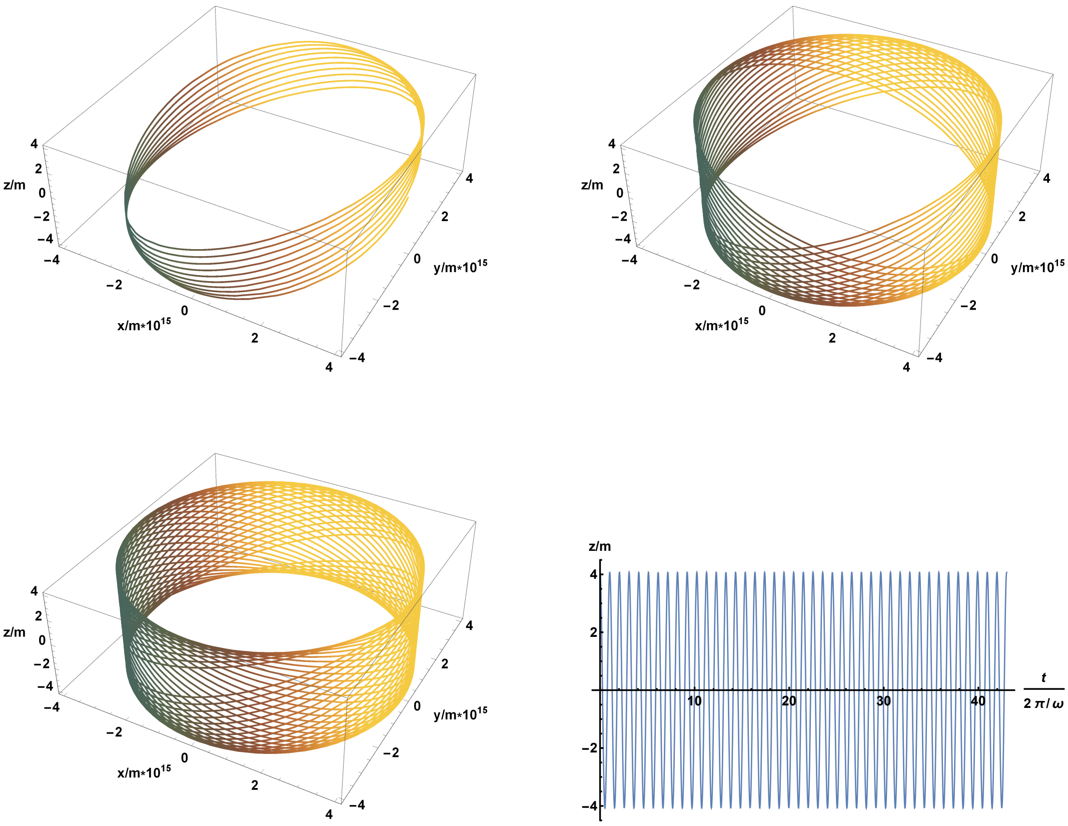

Figure 4.5: Numerical 1PN results for a spinning body in a quasi-circular orbit in a pseudo-isothermal dark matter halo, in what we called the constant amplitude regime. The DM halo has $\rho_0 = 5\times10^7 M_\odot/\mathrm{pc}^3$ and $r_c = 0.02$kpc. The test body is located at $r = 8r_c$ (for which $v = 0.13$) and has $m = M_\odot$ and an initial spin vector with magnitude $S = 0.5m^2$ pointing in the $\boldsymbol{e}_\mathrm{x}$ direction. *From left to right, up down*: Plots of $\{x(t), y(t), z(t)\}$ of the orbit, after $10, 25, 40$ laps; plot of $z(t)$, for $t \in [0, 2\pi/\Omega_\mathrm{s}]$.

2b) "Beating" regime:

Taking $z(0) = \dot{z}(0) = 0$ represents taking a circular orbit, with no initial inclinations. The constants of integration for this choice are $c_1 = -Z$ and $c_2 = 0$. Therefore,

$$z(t) = Z(\cos(\Delta\omega t) - \cos(\sqrt{-G_{z,z}}t)) = Z(\cos(\Delta\omega t) - \cos(\omega t))\,,$$

which we can rewrite, using the trigonometric identity $\cos(b) - \cos(a) = 2\sin\left[\frac{a+b}{2}\right]\sin\left[\frac{a-b}{2}\right]$, as

$$z(t) = 2Z\sin\left[\frac{2\omega - \Omega_{\rm s}}{2}t\right]\sin\left[\frac{\Omega_{\rm s}}{2}t\right]\,. \tag{4.56}$$

The coordinate $z(t)$ will oscillate rapidly with frequency $(2\omega - \Omega_{\rm s})/2$, and its amplitude will be modulated by a wave of frequency $\Omega_{\rm s}/2$ and peak amplitude $2Z$. Since we are considering $\omega \gg \Omega_{\rm s}$, the z frequency of oscillation $(2\omega - \Omega_{\rm s})/2$ is close to the frequency ω.

The 1PN numerical simulations (in which we used the same physical variables as the previous case) are presented in Fig. 4.7. The motion described by equation (4.56) is in accordance with the simulations.

Fig. 4.6 shows the approximated results. Once again, the numerical and the approximated results are in agreement.

Eq. (4.30) tells us that the orbit will precess about the direction of $\boldsymbol{S}$: since the spin vector $\boldsymbol{S}$ is nearly constant in one orbit, i.e. one period, the spin-curvature force (4.41) points in the z direction but changes sign, as the cross product between $\boldsymbol{S}$ and $\boldsymbol{v}$ also changes sign, as seen in Fig. 4.1. Hence, the force 4.41 points in the positive $\boldsymbol{e}_z$ direction for nearly half the orbit, and in the negative for the other half. This will "torque" the orbit, causing it to precess.

For such a system, the maximum amplitude of the z motion is $2Z \approx 1.5 \times 10^5$m, that is about 3×10^{-14} times the motion in the other spatial directions. The orbit inclines about 7×10^4m per lap, which means it takes about 21 laps to reach the maximum inclination. The frequency of the spin precession is $\Omega_{\rm s} \approx 8.9 \times 10^{-14}\text{s}^{-1}$, this means that after $\pi/\Omega_{\rm s} \approx 3.5 \times 10^{14}\text{s} = 1.1 \times 10^6$ yr, the spin direction will be reversed.

Finally, note that the amplitude Z of the z coordinate, given by Eq. 4.51, is proportional to S/m. This quantity is called the Möller radius.

A larger Magnus effect would happen for a system with a higher density, and for a spinning body with a large Möller radius.

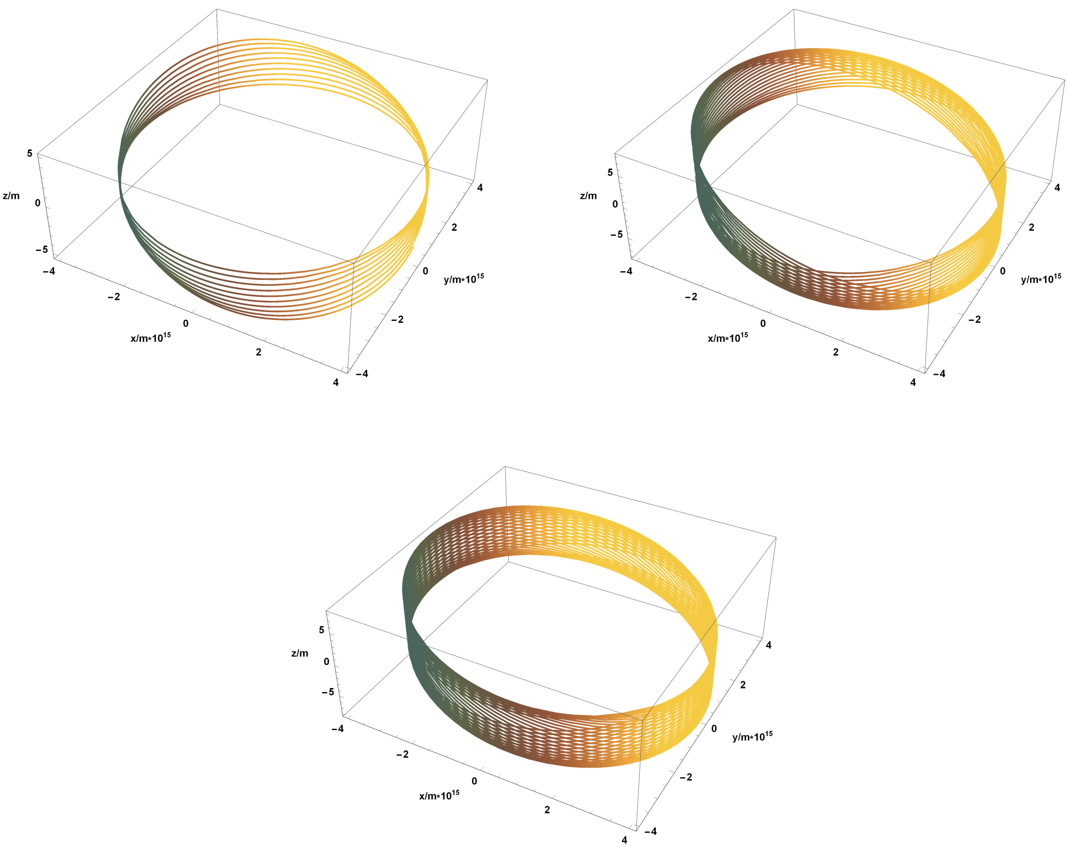

Figure 4.6: Approximated results for a spinning body in a quasi-circular orbit in a pseudo-isothermal dark matter halo, in what we called the “beating” regime. The DM halo has $\rho_0 = 5 \times 10^7 M_\odot/\mathrm{pc}^3$ and $r_c = 0.02$kpc. The test body is located at $r = 8r_c$ (for which $v = 0.13$) and has $m = M_\odot$ and an initial spin vector with magnitude $S = 0.5m^2$ pointing in the $\boldsymbol{e}_\mathrm{x}$ direction. *From left to right, up down*: Plots of $\{x(t), y(t), z(t)\}$ of the orbit, after $10, 25, 40$ laps.

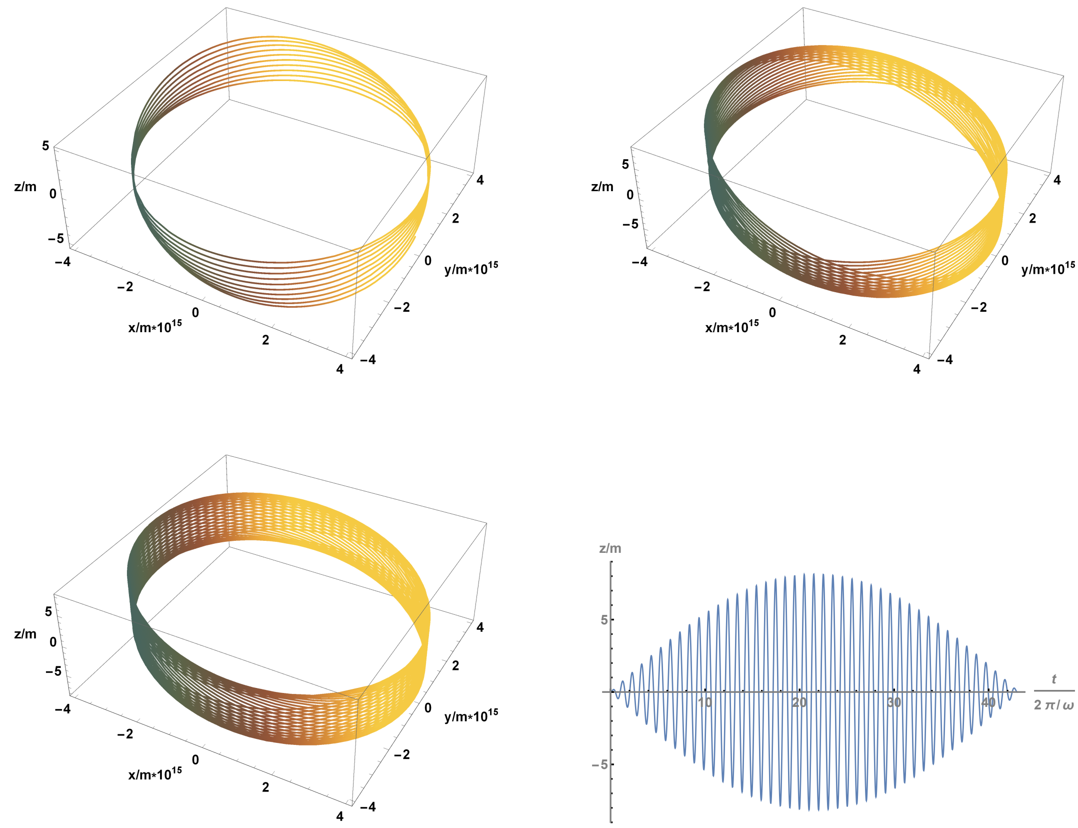

Figure 4.7: Numerical 1PN results for a spinning body in a quasi-circular orbit in a pseudo-isothermal dark matter halo, in what we called the "beating" regime. The DM halo has $\rho_0 = 5 \times 10^7 M_\odot/\mathrm{pc}^3$ and $r_c = 0.02$kpc. The test body is located at $r = 8r_c$ (for which $v = 0.13$) and has $m = M_\odot$ and an initial spin vector with magnitude $S = 0.5m^2$ pointing in the $\boldsymbol{e}_\mathrm{x}$ direction. *From left to right, up down*: Plots of $\{x(t), y(t), z(t)\}$ of the orbit, after $10, 25, 40$ laps; plot of $z(t)$, for $t \in [0, 2\pi/\Omega_\mathrm{s}]$.

Chapter 5

Conclusions

In this thesis, we studied the possibility of the existence of an analogous effect to the fluid dynamics Magnus effect in gravitation. Analogous in the sense that a force arises whenever a spinning body has a non-zero velocity relative to the medium, with this force being orthogonal to the body's spin and on the spatial mass current. A gravitational Magnus-like effect had already been foreshadowed in some literature [49, 50]. Here, we show that indeed a gravitational Magnus force exists, and we studied it for some simple examples.

After briefly discussing the classical fluid dynamics effect, we started the work with an electromagnetic example. We took the force exerted on a dipole placed in an electromagnetic field in terms of the magnetic tidal tensor. Decomposing into its symmetric and antisymmetric parts, we could separate the force into different components. We showed that one of them was an electromagnetic Magnus force, orthogonal to both the particle's magnetic moment and the current density vector. For a positively charged particle, the force pointed in the opposite direction of the classical one; while for a negatively charged particle, the electromagnetic and classical Magnus force pointed in the same direction. In order to correctly establish the comparison between electromagnetism and general relativity and to give more physical intuition to the gravitational case, we introduced the gravitoelectromagnetism formalism.

Afterwards, we studied the spin-curvature force from the equations of motion of a spinning body in a gravitational field. This covariant physical force deviates a spinning body from its geodesic motion. By writing the spin-curvature force in terms of the so called gravitomagnetic tidal tensor and using a similar treatment to the one used in electromagnetism, we recognize two very different components in the spin-curvature force. This approach allowed us to unmask a force that we dubbed gravitational Magnus force F^{α}_{Mag}. This force points in the same direction of the classical one and depends on the same (analogous) quantities and no further detail of the systemand points in the same direction of the classical one. For a spinning particle in a massive medium, this force arises whenever the relative velocity between the body and the medium is not parallel to the body's spin. The other force was dubbed Weyl force since it was due to the magnetic part of the Weyl tensor. We showed that this force has a high dependence on the details of the system such as the boundary conditions.

Without using approximations, the Magnus effect was shown to exist in a FLWR metric - which describes the large scale matter distribution of an homogeneous isotropic Universe. The case is particularly curious since for a particule moving with respect to the background, the only non-vanishing part of the spin-curvature force is the Magnus one. It is the only covariant force that deviates the particle from its geodesic motion. Another particularity is that the force occurs for all forms of energy and mass except for dark energy (when modeled by the cosmological constant). Hence the effects by such a force can also be used as a probe to determine the matter-energy content of the Universe.

Finally, we analized the example of a DM halo, computing the Magnus force on a spinning body moving through the halo. By comparing different density profiles, we confirmed that the Weyl force is highly dependent on the system's details, varying greatly for the different profiles. On the other hand, the Magnus force depends solely on the body's spin, the body's velocity and the local density (given by each profile). The Magnus force led to an interesting secular precession of the orbital plane. These effects could prove to be an independent test of the existence and profile density of DM. The effects were typically small. This is due to the low density of the DM halos, and the effect was more noticeable for test particles with a higher Moller radius S/m.

Another interesting case of the Magnus effect in a more dense astrophysical system is presented in [1], a BH accretion disk. For this example, the effect is more noticeable since the density is also higher. For future work, the Magnus effect could be studied for even more realistic density profiles for both DM and accretion disks. The effects of the Magnus force can also be used as a probe for these profiles, when the detecting technology improves.

Bibliography

[1] L. F. O. Costa, R. Franco, and V. Cardoso. Gravitational magnus effect. 2018.

[2] I. Ciufolini and J. A. Wheeler. *Gravitation and Inertia.* Princeton Univ. Press, Princeton, 1995. ISBN:0-691-03323-4.

[3] R. d'Inverno. *Introducing Einstein's Relativity.* Oxford Univ. Press, Oxford, 1998. ISBN:0-19-859686-3.

[4] C. W. Misner, K. S. Thorne, and J. A. Wheeler. *Gravitation.* W. H. Freeman and Company, San Francisco, 1973. ISBN:.

[5] S. Weinberg. *Gravitation and Cosmology: Principles and applications of the General Theory of Relativity.* John Wiley & Sons, New York, 1972. ISBN: 0-471-92567-5.

[6] D. Bini, P. Carini, R. T. Jantzen, and D. Wilkins. Thomas precession in post-newtonian gravitoelectromagnetism. *Phys. Rev. D*, 49:2820–2827, Mar 1994. doi: 10.1103/PhysRevD.49.2820. URL `https://link.aps.org/doi/10.1103/PhysRevD.49.2820`.

[7] J. D. Kaplan, D. A. Nichols, and K. S. Thorne. Post-newtonian approximation in maxwell-like form. *Phys. Rev. D*, 80:124014, 2009. doi: 10.1103/PhysRevD.80.124014.

[8] V. B. Braginsky, A. G. Polnarev, and K. S. Thorne. Foucault pendulum at the south pole: Proposal for an experiment to detect the earth's general relativistic gravitomagnetic field. *Phys. Rev. Lett.*, 53:863–866, Aug 1984. doi: 10.1103/PhysRevLett.53.863. URL `https://link.aps.org/doi/10.1103/PhysRevLett.53.863`.

[9] R. L. Forward. General relativity for the experimentalist. In *Prooceedings of the IRE*, volume 49, pages 892–904, 1961. doi: 10.1109/JRPROC.1961.287932.

[10] T. Damour, M. Soffel, and C. Xu. General-relativistic celestial mechanics. *Phys. Rev. D*, 43:10, 1991. doi: https://doi.org/10.1103/PhysRevD.43.3273.

[11] R. M. Wald. Gravitational spin interaction. *Phys. Rev. D*, 6:406, 1972. doi: 10.1103/PhysRevD.6.406.

[12] R. T. Jantzen, P. Carini, and D. Bini. Understanding spacetime splittings and their relationships or gravitoelectromagnetism: the user manual. 2004. URL `http://www34.homepage.villanova.edu/robert.jantzen/gem/`.

[13] R. T. Jantzen, P. Carini, and D. Bini. The many faces of gravitoelectromagnetism. *Annals of Physics*, 215:1 – 50, 1992. doi: https://doi.org/10.1016/0003-4916(92)90297-Y.

[14] J. Natário. Quasi-maxwell interpretation of the spin-curvature coupling. *Gen. Rel. Grav*, 39:1477–1487, 2007. doi: https://doi.org/10.1007/s10714-007-0474-7.

[15] L. F. Costa and C. R. Herdeiro. Gravitoelectromagnetic analogy based on tidal tensors. *Phys. Rev. D*, 78:024021, 2008. doi:10.1103/PhysRevD.78.024021.

[16] L. F. Costa, J. Natário, and M. Zilhão. Spacetime dynamics of spinning particles: Exact electromagnetic analogies. *Phys. Rev. D*, 93:104006, 2016. doi:10.1103/PhysRevD.93.104006.

[17] L. F. Costa and J. Natário. Gravito-electromagnetic analogies. *Gen. Relativ. Gravit.*, 46:1792, 2014. doi: 10.1007/s10714-014-1792-1.

[18] M. Mathisson. Republication of: New mechanics of material systems. *Gen. Relativ. Gravit.*, 42: 1011–1048, 2010. doi: 10.1007/s10714-010-0939-y.

[19] A. Papapetrou. Spinning test-particles in general relativity. i. *Proc. R. Soc. Lond. A*, 209:248–258, 1951. doi: 10.1098/rspa.1951.0200.

[20] E. G. Harris. Analogy between general relativity and electromagnetism for slowly moving particles in weak gravitational fields. *Am. J. Phys.*, 59:421, 1991. doi: http://dx.doi.org/10.1119/1.16521.

[21] L. F. Costa and J. Natário. The coriolis field. *Am. J. Phys.*, 84:388, 2016. doi: arXiv:1511.02458.

[22] A. Einstein. Näherungsweise integration der feldgleichungen der gravitation. *Sitzungsberichte der Königlich Preußischen Akademie der Wissenschaften*, 1:688, 1916.

[23] A. Einstein. Über gravitationswellen. *Sitzungsberichte der Königlich Preußischen Akademie der Wissenschaften*, 1:154, 1918.

[24] R. A. Hulse and J. H. Taylor. Discovery of a pulsar in a binary system. *Astrophys. Journal*, 195: L51–L53, 1975. doi: 10.1086/181708.

[25] J. H. Taylor and J. M. Weirsberg. A new test of general relativity: Gravitational radiation and the binary pulsar PSR 1913+16. *Astrophys. Journal*, 253:908–920, 1982. doi: 10.1086/159690.

[26] 2018. URL `https://arstechnica.com/science/2017/02/a-history-of-dark-matter/`.

[27] B. Abbot et al. Observation of gravitational waves from a binary black hole merger. *Phys. Rev. Lett.*, 116:061102, 2016. doi: 10.1103/PhysRevLett.116.061102.

[28] B. Abbot et al. GW151226: Observation of gravitational waves from a 22-solar-mass binary black hole coalescence. *Phys. Rev. Lett.*, 116:241103, 2016. doi: 10.1103/PhysRevLett.116.241103.

[29] B. Abbot et al. GW170817: Observation of gravitational waves from a binary neutron star inspiral. *Phys. Rev. Lett.*, 119:161101, 2017. doi: 10.1103/PhysRevLett.119.161101.

[30] 2018. URL https://www.nobelprize.org/nobel_prizes/physics/laureates/2017.

[31] A. Friedman. Über die krümmung des raumes. *Zeitschrift für Physik*, 10(1):377–386, 1922. doi: 10.1007/BF01332580. URL https://doi.org/10.1007/BF01332580.

[32] G. Lemaître. Un Univers homogène de masse constante et de rayon croissant rendant compte de la vitesse radiale des nébuleuses extra-galactiques. *Annales de la Société Scientifique de Bruxelles*, 47: 49–59, 1927. URL http://adsabs.harvard.edu/abs/1927ASSB...47...49L.

[33] H. P. Robertson. Kinematics and World-Structure. *Astrophys. Journal*, 82:284, 1935. doi: 10.1086/143681. URL http://adsabs.harvard.edu/abs/1935ApJ....82..284R.

[34] W. A. G. On milne's theory of world-structure. *Proceedings of the London Mathematical Society*, s2-42(1):90–127, 1937. doi: 10.1112/plms/s2-42.1.90. URL https://londmathsoc.onlinelibrary.wiley.com/doi/abs/10.1112/plms/s2-42.1.90.

[35] S. Carroll. *Spacetime and geometry - an introduction to General Relativity*. Cambridge Univ. Press, Cambridge, 2012. ISBN: 978-0-521-38115-4.

[36] G. Ellis, R. Maartens, and M. MacCallum. *Relativistic Cosmology*. Cambridge Univ. Press, Cambridge, 2012. ISBN: 978-0-521-38115-4.

[37] J. C. Kapteyn. First Attempt at a Theory of the Arrangement and Motion of the Sidereal System. *Astrophys. Journal*, 55:302, 1922. doi: 10.1086/142670. URL http://adsabs.harvard.edu/abs/1922ApJ....55..302K.

[38] F. Zwicky. Die Rotverschiebung von extragalaktischen Nebeln. *Helvetica Physica Acta*, 6:110–127, 1933. URL http://adsabs.harvard.edu/abs/1933AcHPh...6..110Z.

[39] F. Zwicky. On the masses of nebulae and of clusters of nebulae. *Astrophys. Journal*, 86:217, 1937. doi: 10.1086/143864. URL http://adsabs.harvard.edu/abs/1937ApJ....86..217Z.

[40] V. C. Rubin and W. K. Ford, Jr. Rotation of the andromeda nebula from a spectroscopic survey of emission regions. *Astrophys. Journal*, 159:379, 1970. doi: 10.1086/150317. URL http://adsabs.harvard.edu/abs/1970ApJ...159..379R.

[41] G. Hinshaw, J. L. Weiland, R. S. Hill, N. Odegard, D. Larson, C. L. Bennett, J. Dunkley, B. Gold, M. R. Greason, N. Jarosik, E. Komatsu, M. R. Nolta, L. Page, D. N. Spergel, E. Wollack, M. Halpern, A. Kogut, M. Limon, S. S. Meyer, G. S. Tucker, and E. L. Wright. Five-year wilkinson microwave anisotropy probe observations: Data processing, sky maps, and basic results. *The Astrophysical Journal Supplement Series*, 180(2):225, 2009. URL http://stacks.iop.org/0067-0049/180/i=2/a=225.

[42] M. Velander, E. van Uitert, H. Hoekstra, J. Coupon, T. Erben, C. Heymans, H. Hildebrandt, T. D. Kitching, Y. Mellier, L. Miller, L. Van Waerbeke, C. Bonnett, L. Fu, S. Giodini, M. J. Hudson, K. Kuijken, B. Rowe, T. Schrabback, and E. Semboloni. Cfhtlens: the relation between galaxy

dark matter haloes and baryons from weak gravitational lensing. *Monthly Notices of the Royal Astronomical Society*, 437(3):2111–2136, 2014. doi: 10.1093/mnras/stt2013. URL `http://dx.doi.org/10.1093/mnras/stt2013`.

[43] 2017. URL `https://home.cern/about/physics/dark-matter`.

[44] P. A. R. Ade et al. Planck 2015 results. XIII. Cosmological parameters. *Astron. Astrophys.*, 594: A13, 2016. doi: 10.1051/0004-6361/201525830.

[45] F. M. White. *Fluid Mechanics.* McGraw-Hill, Rhode Island, 4^{th} edition, 1998. ISBN:978-0387303031.

[46] G. Magnus. Über die Abweichung der Geschosse, und: Über eine abfallende Erscheinung bei rotierenden Körpern. *Annalen der Physik*, 164:1–29, 1853. URL `https://gallica.bnf.fr/ark:/12148/bpt6k15173v.pleinepage.r=Annalen+der+Physic.f13.langFR`.

[47] G. Robinson and I. Robinson. The motion of an arbitrarily rotating spherical projectile and its application to ball games. *Phys. Scr.*, 88:018101, 2013. doi: http://iopscience.iop.org/1402-4896/88/1/018101.

[48] H. Chanson. *Applied hydrodynamics: an introduction.* CRC Press, London, 2013. ISBN: 978-0-521-38115-4.

[49] J. A. Font, J. M. Ibáñez, and P. Papadopoulos. Non-axisymmetric relativistic bondi–hoyle accretion on to a kerr black hole. *Mon. Not. R. Astronom. Soc*, 305:920–936, 1999. doi: 10.1046/j.1365-8711.1999.02459.x.

[50] H. Okawa and V. Cardoso. Black holes and fundamental fields: hair, kicks and a gravitational "magnus" effect. *Phys. Rev. D*, 90:104040, 2014. doi:10.1103/PhysRevD.90.104040.

[51] B. Casher, A. Aker, and M. Kesden. Gravitomagnetic dynamical friction. *Phys. Rev. D*, 95:064014, 2017. doi: 10.1103/PhysRevD.95.064014.

[52] D. J. Griffiths. *Introduction to Electrodynamics.* Prentice Hall, New Jersey, 3^{rd} edition, 1999. ISBN:0-13-805326-X.

[53] E. Poisson and C. M. Will. *Gravity - Newtonian, Post-Newtonian, Relativistic.* Cambridge Univ. Press, Cambridge, 2014. ISBN:978-1-107-03286-6.

[54] E. Poisson. *A Relativist's Toolkit.* Cambridge Univ. Press, Cambridge, 2004. ISBN:0-521-83091-5.

[55] S. E. Gralla, A. I. Harte, and R. M. Wald. Bobbing and kicks in electromagnetism and gravity. *Phys. Rev. D*, 81:104012, 2010. doi: 10.1103/PhysRevD.81.104012.

[56] J. F. Costa and J. Natário. Center of mass, spin supplementary conditions and momentum of spinning particles. *Fund. Theor. Phys.*, 179:215–258, 2015. doi:$10.1007/978-3-319-18335-0_6$.

[57] T. Clifton, D. Gregoris, and K. Rosquist. The magnetic part of the weyl tensor and the expansion of discrete universes. *Gen. Rel. Grav.*, 49(2):1–40, 2017. doi: 10.1007/s10714-017-2192-0.

[58] A. Burkert. The structure of dark matter halos in dwarf galaxies. *Astrophys. Journal*, 447:L25–L28, 1995. doi: 10.1086/309560.